

Multi-omic approaches identify metabolic and autophagy regulators important in ovarian cancer dissemination.

Lindsay J Wheeler, Zachary L Watson, Lubna Qamar, Tomomi M Yamamoto, Brandon T Sawyer, Kelly D Sullivan, Santosh Khanal, Molishree Joshi, Véronique Ferchaud-Roucher, Harry Smith, et al.

▶ **To cite this version:**

Lindsay J Wheeler, Zachary L Watson, Lubna Qamar, Tomomi M Yamamoto, Brandon T Sawyer, et al.. Multi-omic approaches identify metabolic and autophagy regulators important in ovarian cancer dissemination.. iScience, 2019, 19, pp.474-491. 10.1016/j.isci.2019.07.049 . hal-02622292

HAL Id: hal-02622292
https://hal.inrae.fr/hal-02622292

Submitted on 26 May 2020

HAL is a multi-disciplinary open access archive for the deposit and dissemination of scientific research documents, whether they are published or not. The documents may come from teaching and research institutions in France or abroad, or from public or private research centers.

L'archive ouverte pluridisciplinaire **HAL**, est destinée au dépôt et à la diffusion de documents scientifiques de niveau recherche, publiés ou non, émanant des établissements d'enseignement et de recherche français ou étrangers, des laboratoires publics ou privés.



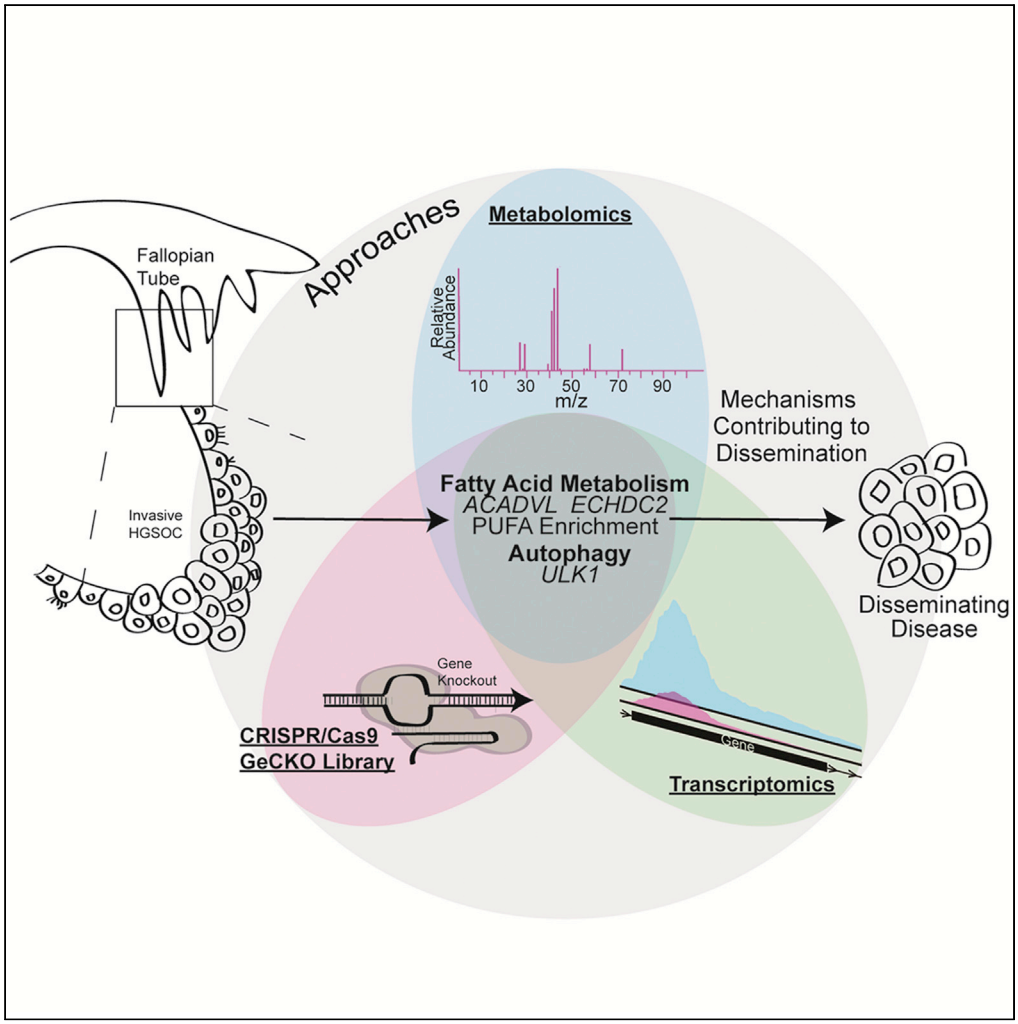
Distributed under a Creative Commons Attribution - NonCommercial - NoDerivatives 4.0 International License

iScience

CellPress

Article

Multi-Omic Approaches Identify Metabolic and Autophagy Regulators Important in Ovarian Cancer Dissemination



Lindsay J. Wheeler, Zachary L. Watson, Lubna Qamar, ..., Joaquin M. Espinosa, Jennifer K. Richer, Benjamin G. Bitler

benjamin.bitler@ucdenver.edu

HIGHLIGHTS

Combined multi-omic screen identifies drivers of ovarian cancer dissemination

Fatty acid metabolism and autophagy identified as drivers of anoikis resistance

Suspension culture of ovarian cancer cells induces metabolic reprogramming

Anoikis resistance gene signature predicts survival in multiple carcinoma types

Wheeler et al., iScience *19*, 474–491
September 27, 2019 © 2019 The Author(s).
https://doi.org/10.1016/j.isci.2019.07.049

iScience

CellPress

Article

Multi-Omic Approaches Identify Metabolic and Autophagy Regulators Important in Ovarian Cancer Dissemination

Lindsay J. Wheeler,[1,9] Zachary L. Watson,[2,9] Lubna Qamar,[2] Tomomi M. Yamamoto,[2] Brandon T. Sawyer,[1] Kelly D. Sullivan,[3,4] Santosh Khanal,[3,4] Molishree Joshi,[3,4] Veronique Ferchaud-Roucher,[1] Harry Smith,[5] Lauren A. Vanderlinden,[5] Sky W. Brubaker,[6] Cecilia M. Caino,[3] Hyunmin Kim,[7] Joaquin M. Espinosa,[3,4] Jennifer K. Richer,[8] and Benjamin G. Bitler[2,10,*]

SUMMARY

High-grade serous ovarian cancers (HGSOCs) arise from exfoliation of transformed cells from the fallopian tube, indicating that survival in suspension, and potentially escape from anoikis, is required for dissemination. We report here the results of a multi-omic study to identify drivers of anoikis escape, including transcriptomic analysis, global non-targeted metabolomics, and a genome-wide CRISPR/Cas9 knockout (GeCKO) screen of HGSOC cells cultured in adherent and suspension settings. Our combined approach identified known pathways, including NOTCH signaling, as well as novel regulators of anoikis escape. Newly identified genes include effectors of fatty acid metabolism, *ACADVL* and *ECHDC2*, and an autophagy regulator, *ULK1*. Knockdown of these genes significantly inhibited suspension growth of HGSOC cells, and the metabolic profile confirmed the role of fatty acid metabolism in survival in suspension. Integration of our datasets identified an anoikis-escape gene signature that predicts overall survival in many carcinomas.

INTRODUCTION

Epithelial ovarian cancer is the deadliest gynecologic malignancy, annually accounting for more than 220,000 deaths worldwide (Jayson et al., 2014). High-grade serous ovarian cancer (HGSOC) comprises the majority of ovarian cancer cases. Although a majority of patients with HGSOC initially respond to first-line therapy, in most patients the cancer will recur within 3 years (Jayson et al., 2014). Achieving optimal surgical resection of the tumors conveys the best prognosis but is challenging given that ovarian cancer, as well as fallopian and primary peritoneal carcinoma, tend to spread to the peritoneal cavity (Berek and Hacker, 2015). As tumor cells spread to the abdominal cavity they lead to the production of ascites, a collection of intraperitoneal fluid containing immune cells, tumor cells, and cytokines, among other cellular and acellular factors (Kim et al., 2016). Tumor cells in ascites are known to be highly invasive, to the extent that a majority of patient-derived xenograft ovarian cancer models are generated from injection of ascites fluid alone, indicating the presence of tumor-initiating cells (Kim et al., 2016; Lengyel et al., 2014). Tumor cells within ascites are thought to be the subpopulation of cells that lead to recurrent or metastatic disease (Kim et al., 2016).

Investigations over the past 10 years have revealed that HGSOC may, in fact, originate from transformed secretory fallopian tube epithelium (FTE) located on the fimbriated end of the fallopian tube. Precursor lesions include serous tubal intraepithelial carcinoma (STIC), which is focal and displays a cytologic appearance similar to HGSOC. HGSOC precursor lesions often exhibit a "p53 signature," which includes normal secretory FTE cells that either lack p53 entirely or overexpress mutant p53 (Lee et al., 2007; Piek et al., 2001, Van Der Steen et al., 2017). Transformed cells within STIC lesions exfoliate from the fallopian tube extracellular matrix (ECM), escape detachment-induced cell death (anoikis), survive in an anchorage-independent manner, and disseminate to the ovary and peritoneum. For most cancers, such as breast and endometrial, anoikis escape followed by intravasation into the circulatory or lymphatic systems are critical steps in the metastatic process. However, ovarian, fallopian, and primary peritoneal carcinomas, or high-grade serous carcinoma of the pelvis, are unique in that cancer cells have direct access to the peritoneal cavity. HGSOC preferentially colonizes the fat-rich omentum, suggesting the metabolic environment contributes to dissemination. Anoikis escape is one of the only properties required by transformed FTE to disseminate.

[1]Division of Gynecologic Oncology, Department of Obstetrics and Gynecology, University of Colorado School of Medicine, Aurora, CO 80045, USA

[2]Division of Reproductive Sciences, Department of Obstetrics and Gynecology, University of Colorado School of Medicine, 12700 E. 19th Avenue, MS 8613, Aurora, CO 80045, USA

[3]Department of Pharmacology, University of Colorado School of Medicine, Aurora, CO 80045, USA

[4]Linda Crnic Institute for Down Syndrome, University of Colorado School of Medicine, Aurora, CO 80045, USA

[5]Department of Biostatistics and Informatics, Colorado School of Public Health, University of Colorado Anschutz Medical Campus, Aurora, CO 80045, USA

[6]Department of Microbiology and Immunology, Stanford University School of Medicine, Stanford, CA 94305, USA

[7]Translational Bioinformatics and Cancer Systems Biology Laboratory, Division of Medical Oncology, Department of Medicine, University of Colorado Anschutz Medical Campus, Aurora, CO 80045, USA

[8]Department of Pathology, University of Colorado School of Medicine, Aurora, CO 80045, USA

[9]These authors contributed equally

[10]Lead Contact

*Correspondence: benjamin.bitler@ucdenver.edu

https://doi.org/10.1016/j.isci.2019.07.049

 © 2019 The Author(s).
This is an open access article under the CC BY-NC-ND license (http://creativecommons.org/licenses/by-nc-nd/4.0/).

In this report, we systematically interrogate the relationship between survival in suspension and anoikis escape and almost every gene in the genome.

Given the limited understanding of the mechanisms promoting ovarian cancer dissemination, we performed a functional CRISPR/Cas9 genome-wide knockout screen to identify critical genes and pathways essential to escape anoikis or promote anchorage-independent survival. In parallel, we evaluated the metabolome and transcriptome (RNA-seq) of HGSOC cells cultured in forced suspension to study anoikis escape. Cross-referencing of the CRISPR/Cas9 knockout screen and global metabolomics revealed genes involved in fatty acid (FA) metabolism and enrichment of poly-unsaturated FAs. Specifically, *ACADVL* or *ECHDC2* promoted poly-unsaturated FA (PUFA) accumulation in suspension cells, and knock down of these genes reduced the viability of cells grown in forced suspension culture. Analysis of the CRISPR/Cas9 knockout screen and RNA-seq data resulted in 108 genes associated with survival in suspension and therefore anoikis escape. Some of these play well-established roles in anchorage-independent survival; for example, NOTCH3 is a known regulator of anoikis escape (Brown et al., 2015). We more closely evaluated 13 ovarian cancer-related genes, including Unc-51 like autophagy activating kinase 1 (*ULK1*), which is a serine/threonine kinase that regulates autophagy (reviewed in Mizushima, 2010). We further examined the expression of the top 108 genes in the context of other cancer types by utilizing gene signature analysis. We cross-referenced the anoikis escape candidate gene list across a variety of carcinoma types, including ovarian, bladder, lung, prostate, breast, colorectal, and brain. We observed that the anoikis escape gene signature predicted overall survival in almost all cancers tested. The data also reveal several novel effectors of anoikis escape, which could be further investigated for therapeutic targeting or prognostic purposes.

RESULTS

CRISPR/Cas9 Screen to Identify Effectors of Anoikis-Escape

During the progression of HGSOC tumor cells must acquire the ability to escape anchorage-independent cell death or anoikis. To identify genes that functionally contribute to anoikis escape we employed a genome-wide CRISPR/Cas9 screening approach in the HGSOC cell line, PEO1. PEO1 cells were selected as the primary cell line because of the HGSOC-like mutational profile (*TP53* and *BRCA2*-mutated), transduction capacity, and moderate growth in suspension. To model HGSOC anoikis escape, cells were forced to grow in suspension by coating tissue culture dishes with poly-2-hydroxyethyl methacrylate (poly-HEMA), which prevents cell attachment and mimics an anchorage-independent microenvironment (Wheeler et al., 2018). PEO1 cells surviving culture on poly-HEMA-coated plates had a low proliferative rate (Figure S1A).

The Genome-Scale CRISPR Knock-Out libraries (GeCKO Libraries A and B, 119,000 individual gRNAs, 6 to 8 gRNA per gene) were lentivirally transduced into PEO1. Multiplicity of infection (MOI) and an effective puromycin concentration were optimized (Figures S1B and S1C). Transduced adherent cells were puromycin selected and allowed to recover. PEO1-GeCKO cells were then plated in adherent or forced suspension settings and harvested after 5 and 10 days (D5 and D10) from both culture conditions in triplicate and genomic DNA was extracted (Figure 1A). To allow for gRNA enrichment or depletion, cells were grown in suspension for 10 days. All samples were sequenced at a depth of at least 25 million reads (Figure S1D).

To identify genes critical for anoikis escape, we determined relative depletion or enrichment for each gRNA in HGSOC cells cultured in suspension conditions (Figure 1B). We focused primarily on day 10 to allow maximum degree of gRNA enrichment or depletion. The data presented represents the comparison of duplicates of Adherent Day 10 (A10) versus Suspension Day 10 (S10), based on principal component analyses and hierarchical clustering (Figures S1E–S1H). Greater than 95% of all genes had at least one gRNA detected (Figure S1I), demonstrating sufficient genome-wide coverage. In the A10 versus S10 comparisons, 15,636 gRNAs representing 11,571 genes were differentially abundant as determined by DESEq2 with Benjamin and Hoschberg multi-testing correction (Figures 1C and 1D). Considering gRNA directionality (enriched or depleted) among the 11,571 genes, there were a total of 2,206 genes with at least two significant targeting gRNAs with similar directionality (Figure 1E). Seventeen genes had four significant gRNA, 219 genes had three significant gRNA, and 1,970 genes had two significant gRNAs (Figure 1E). Functional analysis of the 2,206 genes with gene set enrichment analysis KEGG pathways revealed enrichments in MAPK signaling, focal adhesion, ErbB signaling pathways, and adherence junctions (Table 1). Gene ontology for biological processes related to the 2,206 genes showed significant enrichment in Response to External Stimulus, Regulation of Cell Proliferation, and Regulation of Intracellular Signal Transduction (Table 1). Gene ontology for the molecular function related to the 2,206 genes showed enrichment in Receptor Binding, Signal Transducer Activity, and Signaling Receptor Activity (Table 1). Enrichment analyses

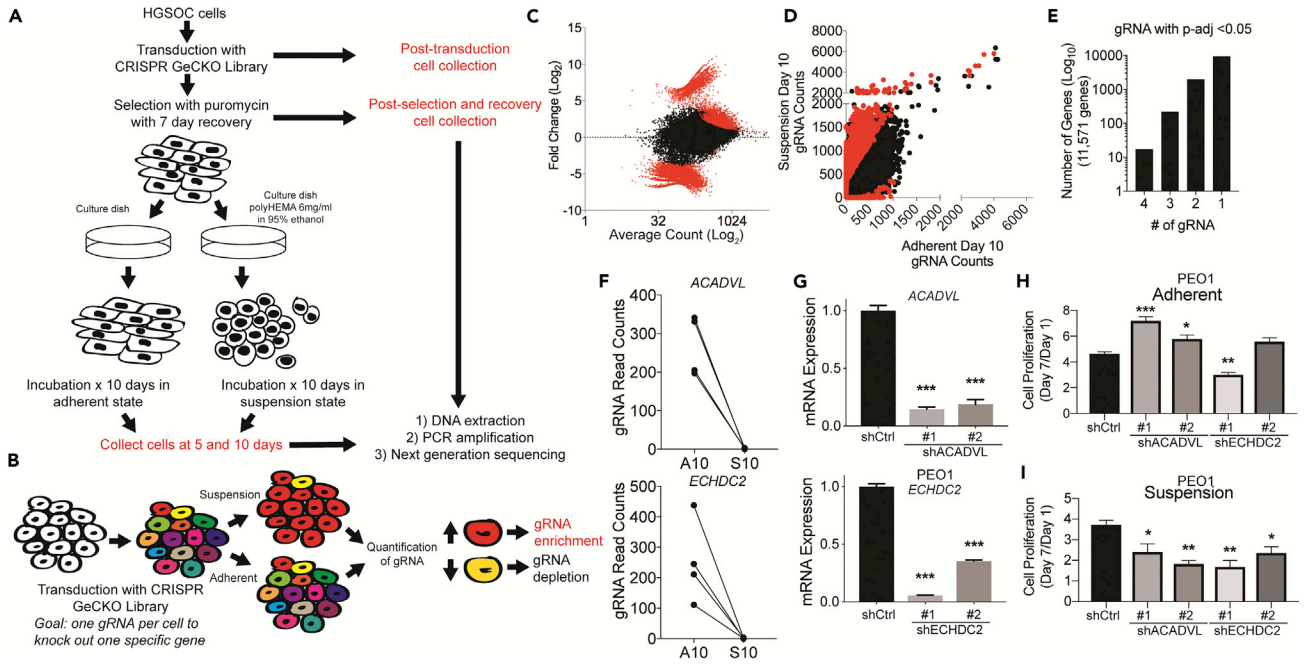


Figure 1. Whole Genome CRISPR/Cas9 Screen to Identify Novel Drivers of Ovarian Cancer Dissemination

(A) Workflow of CRISPR/Cas9 screen. PEO1 cells (HGSOC cells, TP53/BRCA2-mutated) transduced with the Genome-Scale CRISPR Knock-Out (GeCKO) libraries.

(B) Schematic of expected results, which are to identify gRNA enriched (red) or depleted (yellow) in PEO1 cells grown in suspension.

(C) Scatterplot (dot = 1 single gRNA) of Fold Change (Suspension/Adherent, x axis) and average gRNA count (y axis). Red dots = Adjusted p value < 0.05.

(D) Scatterplot of gRNAs from Adherent Day 10 (x axis) and Suspension Day 10 (y axis). Red dots = gRNA with adjusted p < 0.05.

(E) The number of significant (adj. p < 0.05) gRNA with the same directionality associated with a gene.

(F) Significant (adj. p < 0.05) *ACADVL* or *ECHDC2*-specific gRNA in PEO1 cells and their respective change in abundance between adherent day 10 (A10) and suspension day 10 (S10).

(G) PEO1 cells were transduced with shControl (shCtrl) or shACADVL (#1 and #2) or shECHDC2 (#1 and #2). RNA was extracted from cells and used for RT-qPCR against *ACADVL* and *ECHDC2*. Internal control = 18S.

(H) Same as G, but cells were plated on tissue culture treated plastic (adherent) on day 0. Double-stranded DNA content was used as a surrogate for cell number and was measured on day 1 and day 7. Y axis represents the change in cell number from Day 1 to Day 7.

(I) Same as H, cells were plated in low adherent tissue culture plates (suspension), and double-stranded DNA content was measured on day 1 and day 7. Y axis represents the change in cell number from Day 1 to Day 7. Statistical test = ANOVA.

*p < 0.05, **p < 0.01, ***p < 0.001. Error bars = S.E.M. See also Figure S1.

suggest a contribution of receptor tyrosine kinase signaling and external stimuli driving intracellular signaling in anoikis escape.

Sixteen of the 17 genes with four significant (adj. p value < 0.05) gRNAs shared directionality and were depleted in S10 compared with A10, suggesting that the targeted genes are required for survival in the context of anchorage independence. Examining the top 17 genes using functional analysis failed to identify any enriched significant pathways; however, two of the 17 genes are associated with fatty acid metabolism. Four gRNAs specific for acyl-CoA dehydrogenase, very long chain (*ACADVL*) and Enoyl-CoA Hydratase Domain Containing 2 (*ECHDC2*) were depleted in S10 compared with A10 (Figure 1F). *ACADVL* promotes β-oxidation of long-chain fatty acids (FAs) (Kurtz et al., 1998), and *ECHDC2* is involved in FA biosynthesis (Bahnson et al., 2002). In The Cancer Genome Atlas of ovarian cancer, *ECHDC2* and *ACADVL* have a strong positive correlation (Spearman r = 0.25, p = 8.1×10^{-6}, q = 1.655×10^{-4}) suggesting that both genes are upregulated within the same tumor. The primary site of HGSOC dissemination is the fat-rich omentum, which has high levels of FA, including linoleic acid. These findings and previous reports suggest FA metabolism potentiates HGSOC dissemination (Liu et al., 2015; Miranda et al., 2016).

We further confirmed *ACADVL* and *ECHDC2* are important in regulating anoikis escape through small hairpin knockdown (shRNA). We transduced PEO1 and OVCAR4 cell lines with a control plasmid (shCtrl) or two independent shRNA for either *ACADVL* or *ECHDC2*. Both shRNAs for *ACADVL* and *ECHDC2*

Gene Set Name	# Genes in Gene Set (K)	# Genes in Overlap (k)	k/K	p Value	FDR Q-Value
KEGG					
Pathways in cancer	328	54	16.5%	4.47×10^{-17}	8.32×10^{-15}
Focal adhesion	201	35	17.4%	2.67×10^{-12}	2.48×10^{-10}
Mapk signaling pathway	267	40	15.0%	1.08×10^{-11}	6.71×10^{-10}
Erbb signaling pathway	87	20	23.0%	8.10×10^{-10}	3.63×10^{-8}
Calcium signaling pathway	178	29	16.3%	9.77×10^{-10}	3.63×10^{-8}
Endometrial cancer	52	15	28.9%	3.62×10^{-9}	1.12×10^{-7}
Chemokine signaling pathway	190	29	15.3%	4.59×10^{-9}	1.22×10^{-7}
Adherens junction	75	17	22.7%	1.86×10^{-8}	3.85×10^{-7}
B cell receptor signaling pathway	75	17	22.7%	1.86×10^{-8}	3.85×10^{-7}
Insulin signaling pathway	137	23	16.8%	2.87×10^{-8}	5.33×10^{-7}
GO Biological Processes					
Phosphate-containing compound metabolic process	1,977	245	12.4%	2.47×10^{-50}	1.10×10^{-46}
Response to external stimulus	1,821	229	12.6%	4.74×10^{-48}	1.05×10^{-44}
Regulation of transport	1,804	227	12.6%	1.15×10^{-47}	1.70×10^{-44}
Positive regulation of gene expression	1,733	217	12.5%	3.45×10^{-45}	3.83×10^{-42}
Protein localization	1,805	222	12.3%	5.69×10^{-45}	5.05×10^{-42}
Positive regulation of response to stimulus	1,929	231	12.0%	7.09×10^{-45}	5.24×10^{-42}
Positive regulation of biosynthetic process	1,805	220	12.2%	6.30×10^{-44}	3.99×10^{-41}
Response to endogenous stimulus	1,450	192	13.2%	1.98×10^{-43}	1.10×10^{-40}
Regulation of cell proliferation	1,496	193	12.9%	5.22×10^{-42}	2.57×10^{-39}
Regulation of intracellular signal transduction	1,656	204	12.3%	2.20×10^{-41}	9.74×10^{-39}

Table 1. Pathway Analysis of Significant Genes Identified with CRISPR/Cas9 Screen

(Continued on next page)

Gene Set Name	# Genes in Gene Set (K)	# Genes in Overlap (k)	k/K	p Value	FDR Q-Value
GO Molecular Function					
Ribonucleotide binding	1,860	225	12.1%	2.10×10^{-44}	1.89×10^{-41}
Adenyl nucleotide binding	1,514	197	13.0%	1.96×10^{-43}	8.81×10^{-41}
Receptor binding	1,476	185	12.5%	1.54×10^{-38}	4.64×10^{-36}
Enzyme binding	1,737	193	11.1%	5.23×10^{-33}	1.18×10^{-30}
Receptor activity	1,649	185	11.2%	3.52×10^{-32}	6.35×10^{-30}
Kinase activity	842	118	14.0%	3.97×10^{-29}	5.97×10^{-27}
Signal transducer activity	1,731	183	10.6%	1.21×10^{-28}	1.56×10^{-26}
Molecular function regulator	1,353	156	11.5%	1.72×10^{-28}	1.94×10^{-26}
Transferase activity transferring phosphorus-containing groups	992	125	12.6%	1.93×10^{-26}	1.93×10^{-24}
Protein kinase activity	640	91	14.2%	3.63×10^{-23}	3.27×10^{-21}

Table 1. *Continued*
Related to Figure 1.

knocked down the mRNA expression of the target gene (Figures 1G and S1J). In adherent and suspension cell culture conditions over 7 days, we measured DNA double strand content as a surrogate for cell number of shCtrl, shACADVL, or shECHDC2 cells. In the adherent setting, PEO1 *ACADVL* knockdown cells slightly increased cell number, whereas in OVCAR4 *ACADVL* knockdown cells did not have an effect (Figures 1H and S1K). In adherent *ECHDC2* knockdown PEO1 and OVCAR4 cells, proliferation was reduced in one of the two shRNA compared with shCtrl (Figures 1H and S1K). In suspension culture, both *ACADVL* and *ECHDC2* knockdown in PEO1 and OVCAR4 cells significantly decreased cell number compared with shCtrl (Figures 1I and S1L). These results provide confidence that the CRISPR/Cas9 screen identified suspension-related genes and highlight the importance of two metabolic enzymes.

Global Metabolomics Confirms Metabolic Alterations in Anoikis-Resistant Cells

Relative levels of metabolites were examined in adherent versus suspension cultured PEO1 cells via global non-targeted metabolomics, which is a powerful mass-spectrometry-based approach to assess the metabolic profile in a non-biased fashion (Figure 2A and Table S1). Notably, 15 of the 35 detected FA metabolites were significantly ($p < 0.05$) enriched in cells grown in suspension cells (Figure 2B). In an independent cell line (OVARY1847, *TP53*-mutated, *BRCA* wild-type) global non-targeted metabolomics demonstrated 19 of 35 detected FA metabolites enriched in cells grown in suspension compared with adherent cells (Figure S2A and Table S1). Enriched FA between PEO1 and OVARY1847 significantly overlapped, highlighting that the accumulation of FA in anoikis-escaped cells is not cell-line dependent (Figure 2C). We observed differences between PEO1 and OVARY1847 cells, particularly in acyl-carnitine metabolites. For example, two short-chain acyl-carnitine metabolites (propionyl and butanoyl carnitine) are decreased only in PEO1, whereas three medium chain are increased in PEO1 against five in OVARY1847 (from hexanoyl-L-carnitine to O-tetradecanoyl-carnitine). These data suggest that the rate-limiting step of FA β-oxidation mediated by carnitine palmityltransferase is differently regulated in PEO1 suspension compared with OVARY1847 suspension. Both PEO1 and OVARY1847 cells in suspension are enriched for long- and very-long-chain fatty acids, specifically poly-unsaturated FA (e.g., linoleic acid) compared with adherent cells. In PEO1 and OVARY1847 cells grown in suspension, linoleic acid was enriched when compared with adherent cells,

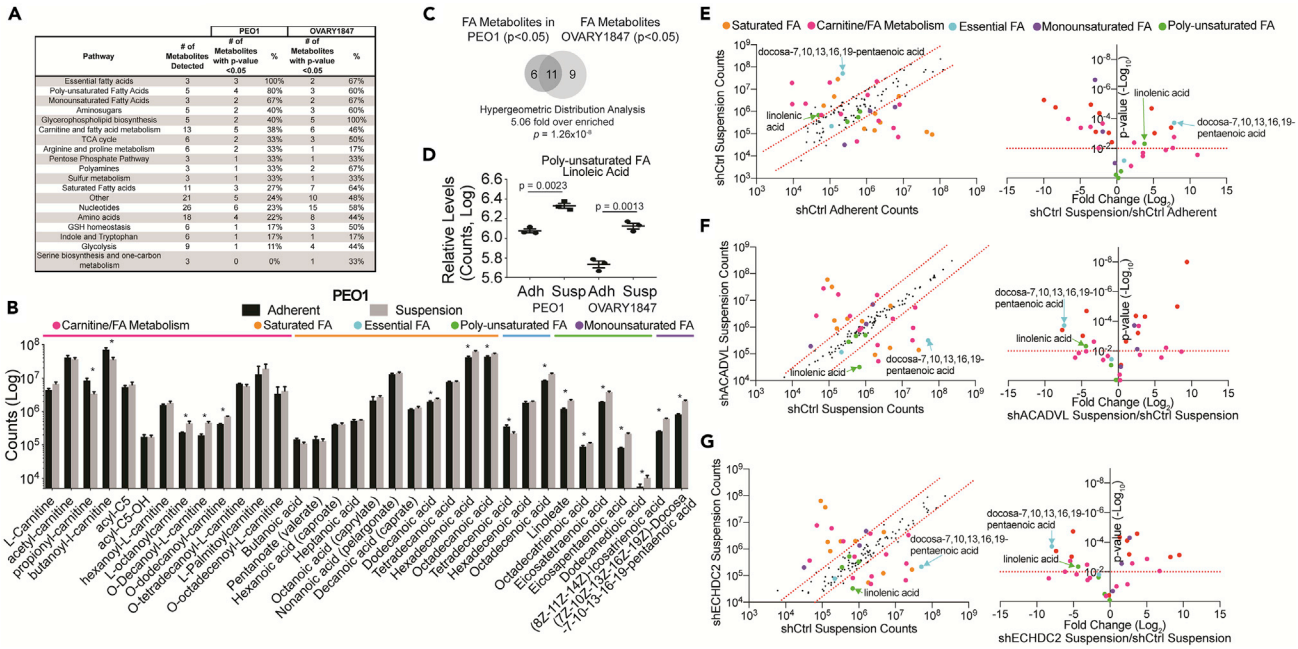


Figure 2. HGSOC Cells Cultured in Suspension Are Enriched for Fatty Acids and Fatty Acid Metabolites

HGSOC cells (PEO1 and OVARY1847) were cultured in adherent and suspension cultures for 48 h. Cells were collected and used for global non-targeted metabolomics.

(A) Metabolites grouped based on pathway. The number of significant ($p < 0.05$) metabolites indicated with percentage (%) of pathway. See Table S1 for a full list of metabolites.

(B) Fatty acids and fatty acids metabolites in PEO1 cells grown in adherent (black bars) or suspension (gray bars) conditions. *p value < 0.05.

(C) Comparison of differentially enriched fatty acids and fatty acid metabolites in PEO1 versus OVARY1847.

(D) An example of poly-unsaturated fatty acids enriched in PEO1 and OVARY1847 suspension cells.

(E) Global non-targeted metabolomics analysis of shCtrl PEO1 cells cultured in adherent versus suspension. Left Panel, metabolite counts graphed as a scatterplot. x axis, shCtrl adherent and y axis, shCtrl suspension. Right Panel, x axis, Log2-Fold change of metabolites and y axis, p value.

(F) Metabolomics analysis of shCtrl PEO1 cells cultured in suspension versus shACADVL cells cultured in suspension. Left Panel, metabolite counts graphed as a scatterplot. x axis, shCtrl suspension and y axis, shACADVL suspension. Right Panel, x axis, Log2-Fold change of metabolites and y axis, p value.

(G) Metabolomics analysis of shCtrl PEO1 cells cultured in suspension versus shECHDC2 cells cultured in suspension. Left Panel, metabolite counts graphed as a scatterplot. x axis, shCtrl suspension and y axis, shECHDC2 suspension. Right Panel, x axis, Log2-Fold change of metabolites and y axis, p value. Red dotted lines indicated p value threshold. Statistical test = unpaired t test. Error bars = S.E.M.

See also Figure S2.

which was validated in an independent experiment (Figures 2D and S2B). These data suggest that cells grown in suspension accumulate PUFAs as a potential metabolic adaptation to resist anoikis.

In the CRISPR/Cas9 screen analysis, two of the top hits were involved in FA metabolism, *ACADVL* and *ECHDC2*. Loss of either enzyme reduces the viability of cells grown in suspension culture (Figure 1I). ACADVL promotes β-oxidation of FA and ECHDC2 contributes to FA biosynthesis, thus these enzymes function at different aspects of FA metabolism. We therefore wanted to assess the metabolic profile of suspension cells following the knockdown of either *ACADVL* or *ECHDC2*. Relative levels of metabolites were examined in adherent versus suspension cultured shCtrl PEO1 and shACADVL or shECHDC2 cells via global non-targeted metabolomics (Table S2). We confirmed that PUFAs are enriched in shCtrl suspension cells compared with shCtrl adherent cells (Figure 2E). *ACADVL* or *ECHDC2* knockdown (Figure 1G) cells cultured in suspension led to the significant depletion of PUFAs in suspension cells (Figures 2F and 2G). Notably, *ACADVL* or *ECHDC2* knockdown cells cultured in suspension displayed similar metabolic profiles (Figures S2C and S2D). Taken together, these data indicate that ACADVL or ECHDC2 has distinct functions in FA metabolism, and loss of either enzyme leads to the depletion of PUFAs in suspension cultured cells.

Anoikis Resistance Associated Transcriptome

The CRISPR/Cas9 KO screen interrogated the loss of individual genes and the ability of HGSOC cells to remain viable in suspension. In non-transduced PEO1 cells a sub-population of cells survive under forced

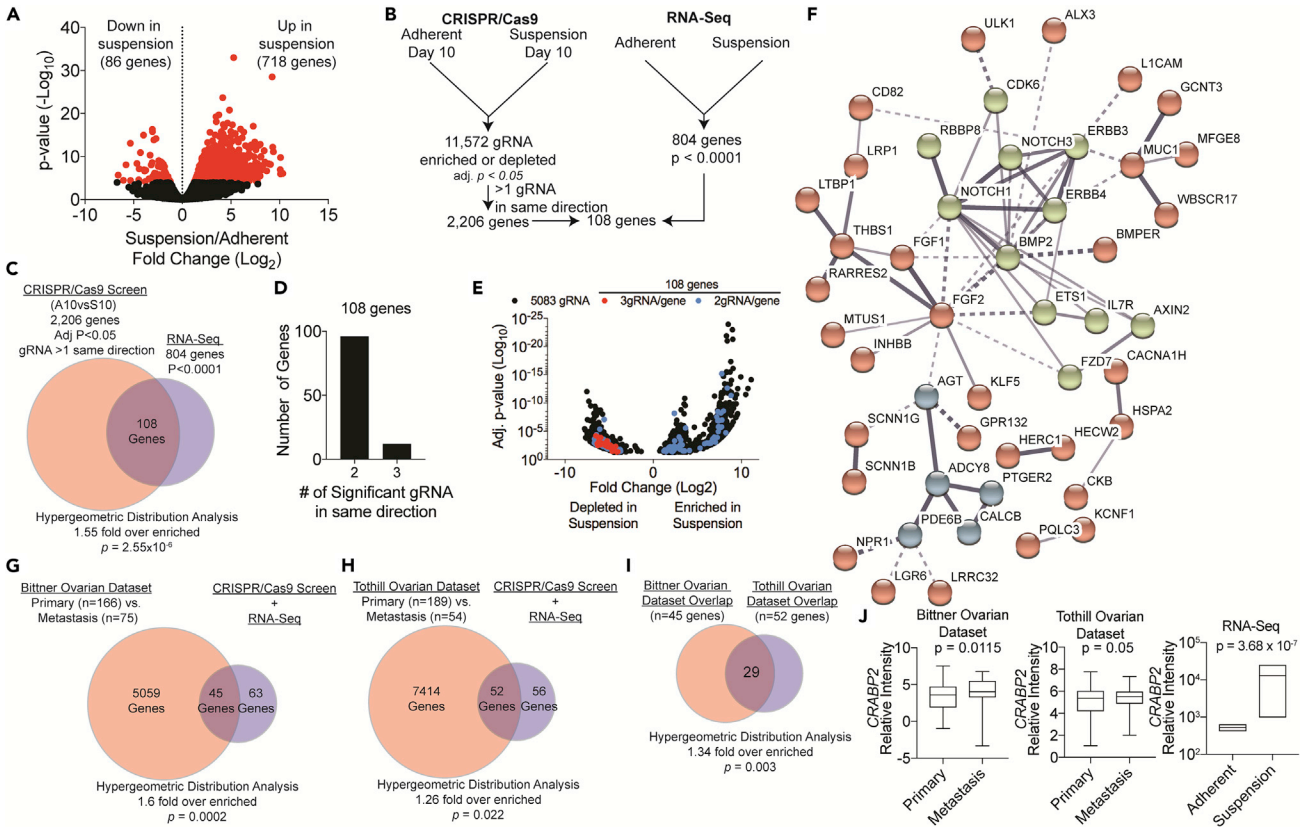


Figure 3. Suspension-Dependent Transcriptomic Changes Are Associated with Metastatic HGSOC

(A) PEO1 cells were grown in adherent or suspension cultures for 10 days. RNA was extracted from cells and utilized for RNA-sequencing. Scatterplot of Fold Change (Log2, x axis) comparing p value (Log10, y axis). Red dots are 804 differentially regulated genes ($p < 0.0001$).

(B) Workflow on combining RNA-Seq and CRISPR/Cas9 datasets.

(C) Overlapped genes identified from CRISPR/Cas9 and RNA-seq analyses before thresholding directionality of gRNA.

(D) Number of gRNA for 108 genes.

(E) Scatterplot of the gRNAs associated with 2,206 genes identified from CRISPR/Cas9 criteria. Fold change of most significant gRNA (x axis) compared with adjusted p value (y axis). Red dots (3 gRNAs) and blue dots (2 gRNA) indicate 108 genes that overlapped with RNA-seq.

(F) Protein-protein interaction (STRING) analysis of 108 genes. Disconnected nodes are hidden. Line thickness correlates to confidence of protein-protein interaction.

(G) Overlap analysis of 108 genes with differentially expressed genes in primary (n = 166) versus metastatic (n = 75) ovarian adenocarcinoma from the Bittner Ovarian Cancer Dataset.

(H) Overlap analysis of 108 genes with differentially expressed genes in primary (n = 189) versus metastatic (n = 54) ovarian adenocarcinoma from the Tothill Ovarian Cancer Dataset.

(I) Overlap analysis of common genes identified in (G) and (H).

(J) *CRABP2* expression in metastatic versus primary HGSOC tumors from G and H, and PEO1 cells adherent versus suspension cells. p Values = unpaired t test. Error bars = S.E.M.

See also Figure S3.

suspension culture. Therefore, to assess transcriptional adaptations that allow for suspension survival and to cross-reference genes identified in CRISPR/Cas9 KO screen, we examined the transcriptome of PEO1 cells that survive under suspension culture conditions for 10 days. Principal component analysis and hierarchal clustering showed that the "Adherent" and "Suspension" samples grouped (Figures S3A and S3B). Comparing the transcriptome of the adherent to suspension cells, we identified 804 differentially expressed genes ($p < 0.0001$; Figure 3A and Table S3). We found 718 upregulated and 86 downregulated genes associated with suspension culture. Although not statistically significant the CRISPR/Cas9 screen hits *ACADVL* and *ECHDC2* were upregulated 1.14X and 1.86X, respectively. Notably, the most significant differentially expressed gene was *MUC16* (Log2 FC = 5.29, False Discovery Rate = 1.85×10^{-29}), which was upregulated in cells in suspension culture. MUC16 is known as cancer antigen 125 (CA125), which is routinely used as a biomarker in the clinic to monitor HGSOC progression.

KEGG pathway analysis of the 804 genes differentially regulated in anoikis-resistant cells revealed enriched pathways including focal adhesion, ECM-receptor interaction, TGFβ-signaling, cell adhesion molecules, and arachidonic acid metabolism (Table 2). KEGG pathway enrichment for arachidonic acid (a PUFA) metabolism highlights an overlap between the CRISPR/Cas9 screen, metabolomics, and RNA-sequencing analysis. Gene ontology for biological processes related to the 804 genes showed significant enrichment for tissue development, regulation of cell proliferation, and positive regulation of response to stimulus (Table 2). Gene ontology for the molecular function related to the 804 genes showed enrichment for receptor binding and activity, signal transducer activity, and transmembrane transporter activity (Table 2). The combined –omics approaches indicate a role of PUFA metabolism in conveying a survival advantage for cells cultured in suspension. Independent of the metabolomics, we further investigated the overlap between the CRISPR/Cas9 screen and RNA-seq analysis.

CRISPR/Cas9 Screen Combined with Transcriptome

Genes identified in the CRISPR/Cas9 screen (2,206 genes) were compared with the RNA-seq differentially expressed genes (804 genes) (Figure 3B), which showed a significant overlap of 108 genes (Hypergeometric test, $p = 2.55 \times 10^{-6}$; Figures 3C and Table S4). Overall, within the 108 genes that overlapped within the datasets, 96 genes had two gRNAs and 12 genes had three gRNAs (Figure 3D). Within the 108 genes, we did not detect genes involved in FA metabolism, highlighting potential differences in essential (CRISPR/Cas9) and sufficient (RNA-seq) genes. These 108 genes had gRNAs that were distributed between being enriched or depleted in suspension cultures conditions (Figure 3E), and notably 10 of 12 genes with the three-gRNA genes were significantly upregulated in suspension (Table S4). KEGG pathway analysis of these 108 genes revealed enriched pathways including pathways in cancer, dorsoventral axis formation (Notch signaling), and TGFβ signaling (Table 3). Gene ontology for biological processes related to the 108 genes showed significant enrichment for tissue development, regulation of cell differentiation, and positive regulation of developmental process (Table 3). Gene ontology for molecular function related to the 108 genes showed enrichment of receptor binding and activity, and transporter activity (Table 3). Protein-protein network interaction analysis on the 108 genes was conducted (Szklarczyk et al., 2017). Protein-protein network analysis and kMeans clustering identified three distinct protein-protein interaction clusters: NOTCH, TGFβ, and ERBB receptor signaling, receptor-ligand interactions, and intracellular signaling (Figure 3F). Although FA metabolic pathways were not enriched in the 108 CRISPR/RNA-seq gene set, NOTCH, TGFβ, and ERBB signaling regulate FA uptake, activate transcription of FA metabolism genes, and promote FA synthesis, respectively (Bian et al., 2015; Jabs et al., 2018; Soukupova et al., 2017). The high degree of concordance between the two (CRISPR/Cas9 screen and RNA-seq) independent genomic datasets and the previously described pathways provide confidence in the findings.

Clinical Relevance

Anoikis escape during ovarian cancer dissemination is a part of the metastatic process; therefore, we next examined the 108 top identified genes against published ovarian cancer datasets that evaluated primary and metastatic (disseminated) disease. The Bittner Ovarian Dataset (GEO: GSE2109) with human genome microarray examined 241 patients with ovarian carcinoma and included both primary tumors (n = 166) and metastatic tumors (n = 75). Comparing primary and metastatic tumors, 5,104 genes were differentially regulated and significantly 45 of our 108 top genes overlapped (Figure 3G, p = 0.0002). The Tothill Ovarian Cohort (GEO: GSE9899) examined 243 patients with ovarian carcinoma including both primary tumors (n = 189) and metastatic tumors (n = 54). Comparing primary versus metastatic tumors, 7,466 genes were differentially regulated and significantly 52 of 108 top hits overlapped (Figure 3H, p = 0.022). On examination of the level of congruency between the genes that overlapped within the metastatic signatures of both datasets we observed that 29 genes overlapped, representing a significant (p = 0.003) enrichment (Figure 3I and Table S5). Examination of expression directionality within these 29 genes found 10 genes that shared directionality between all of the datasets. For example, Cellular Retinoic Acid Binding Protein 2 (*CRABP2*) was upregulated in all of the datasets (Figure 3J) and is a biomarker for ovarian cancer (Toyama et al., 2012). Furthermore, we examined the expression of the 108 genes in matched primary tumor, ascites tumor cells, and metastatic tumors from five patients with ovarian cancer (GEO: GSE73064) (Gao et al., 2019). Of the 108 genes, there were 41 genes that were expressed in a similar direction (Table S6, Columns D-I). These data highlight that the 108 genes identified through –omics approaches are relevant and relatable to disseminated and metastatic ovarian cancer clinical specimens.

Gene Set Name	# Genes in Gene Set (K)	# Genes in Overlap (k)	k/K	p Value	FDR Q-Value
KEGG					
Pathways in cancer	328	26	7.9%	7.97×10^{-11}	1.48×10^{-8}
Focal adhesion	201	17	8.5%	5.76×10^{-8}	5.36×10^{-6}
Dilated cardiomyopathy	92	11	12.0%	4.06×10^{-7}	2.52×10^{-5}
ECM-receptor interaction	84	10	11.9%	1.42×10^{-6}	5.48×10^{-5}
Hypertrophic cardiomyopathy (HCM)	85	10	11.8%	1.59×10^{-6}	5.48×10^{-5}
TGF-beta signaling pathway	86	10	11.6%	1.77×10^{-6}	5.48×10^{-5}
Complement and coagulation cascades	69	9	13.0%	2.20×10^{-6}	5.85×10^{-5}
Cell adhesion molecules (CAMs)	134	12	9.0%	2.79×10^{-6}	6.48×10^{-5}
Regulation of actin cytoskeleton	216	15	6.9%	4.09×10^{-6}	8.46×10^{-5}
Arachidonic acid metabolism	58	8	13.8%	5.28×10^{-6}	9.82×10^{-5}
GO Biological Processes					
Tissue development	1,518	138	9.1%	1.12×10^{-60}	4.98×10^{-57}
Regulation of multicellular organismal development	1,672	138	8.3%	1.45×10^{-55}	3.21×10^{-52}
Positive regulation of developmental process	1,142	103	9.0%	1.23×10^{-44}	1.82×10^{-41}
Epithelium development	945	94	10.0%	2.79×10^{-44}	3.09×10^{-41}
Regulation of cell proliferation	1,496	116	7.8%	9.54×10^{-44}	8.46×10^{-41}
Regulation of anatomical structure morphogenesis	1,021	94	9.2%	1.87×10^{-41}	1.38×10^{-38}
Regulation of cell differentiation	1,492	111	7.4%	3.89×10^{-40}	2.46×10^{-37}
Positive regulation of multicellular organismal process	1,395	106	7.6%	4.00×10^{-39}	1.99×10^{-36}
Positive regulation of response to stimulus	1,929	125	6.5%	4.05×10^{-39}	1.99×10^{-36}
Neurogenesis	1,402	106	7.6%	6.26×10^{-39}	2.78×10^{-36}
GO Molecular Function					
Receptor binding	1,476	107	7.3%	1.16×10^{-37}	1.05×10^{-34}
Molecular function regulator	1,353	82	6.1%	9.58×10^{-24}	4.32×10^{-21}
Receptor activity	1,649	90	5.5%	7.09×10^{-23}	2.13×10^{-20}
Signal transducer activity	1,731	90	5.2%	1.82×10^{-21}	4.10×10^{-19}
Transporter activity	1,276	74	5.8%	2.11×10^{-20}	3.80×10^{-18}
Transmembrane transporter activity	997	63	6.3%	2.50×10^{-19}	3.75×10^{-17}
Enzyme binding	1,737	86	5.0%	3.28×10^{-19}	4.22×10^{-17}

Table 2. Pathway Analysis of Significant Genes Identified with RNA-Sequencing

(Continued on next page)

Gene Set Name	# Genes in Gene Set (K)	# Genes in Overlap (k)	k/K	p Value	FDR Q-Value
Sequence specific DNA binding	1,037	61	5.9%	2.84×10^{-17}	3.20×10^{-15}
Calcium ion binding	697	49	7.0%	4.22×10^{-17}	4.22×10^{-15}
RNA polymerase II transcription factor activity sequence specific DNA binding	629	46	7.3%	8.93×10^{-17}	8.05×10^{-15}

Table 2. *Continued*
Related to Figure 3.

Validation and Ovarian Cancer Relevance

To validate a subset of the 108 genes identified in the RNA-seq and CRISPR/Cas9 comparisons, The Protein Atlas database (Uhlen et al., 2010, 2015) was used to examine tissue and pathologic expression of the genes (Table S6, Columns J-K). We identified genes that are predominantly expressed in ovarian cancer compared with 16 other cancer types. Furthermore, we cross-referenced the 108 genes to differentially regulated genes in a dataset that examined fallopian tube epithelium (FTE) cells in adherent and suspension (GEO: GSE51220 [Lawrenson et al., 2013]) (Table S6, Columns L-M). Lastly, expression of the 108 genes was examined in a dataset that compared normal FTE with high-grade serous carcinoma; 46 of 108 were significantly differentially regulated (GEO: GSE10971 [Tone et al., 2008]) (Table S6, Columns N-O). Based on the Protein Atlas and FTE datasets we selected 13 genes to confirm their role in anoikis escape (Figure 4A). Of 13 genes, 12 shared directionality between FTE and PEO1 cells grown in suspension, with the exception of Retinoblastoma Binding Protein 8 (*RBBP8*), which was downregulated in FTE cells. In the PEO1 RNA-seq analysis, all 13 genes were differentially upregulated in suspension and we validated the expression of these genes (Figure 4B). In contrast, OVCAR4 grown under adherent and suspension conditions displayed a slightly different expression profile. In OVCAR4, 8 of 13 genes were differentially expressed in suspension compared with adherent cells (Figure S4A). The gRNA profile for each gene demonstrated that all had gRNA depletion when cells were cultured in suspension, suggesting these genes are required for anchorage-independent cell survival (Figure 4C).

These 13 genes potentially contribute to HGSOC cell survival in suspension, so we assessed cell viability following the knock down of each gene. Two independent shRNAs for each gene were pooled together, and PEO1 and OVCAR4 cells were transduced with the control shRNA or pooled shRNA. Gene knockdown was evaluated and confirmed with quantitative RT-PCR (RT-qPCR) (Figures 4D and S4B). In both PEO1 and OVCAR4 cells, 10 of 13 genes were significantly downregulated (Figures 4D and S4B). In PEO1 and OVCAR4 knockdown cells, we assessed growth in adherent and suspension settings. Double-stranded DNA content was measured as a surrogate for cell viability. In PEO1, 9 of 10 knockdowns had reduced viability in suspension compared with adherent (Figures 4E–4G). Knockdown of *LGR6* was the exception, which showed increased cell viability in suspension compared with cells grown in adherent conditions (Figure 4G). In OVCAR4, only the 10 genes with significant knockdown resulted in decrease anchorage-independent cell growth, highlighting a direct correlation between the level of gene knockdown and suspension growth (Figures S4C and S4D). Taken together, most of the 13 genes selected for validation were confirmed to be important in maintaining cell viability when cells were cultured in suspension.

In both PEO1 and OVCAR4 cell lines, knockdown of *ULK1* showed the most significant loss of cell viability in cells cultured in suspension over cells in adherent conditions. We next assessed whether suspension induced autophagy. Autophagy was assessed with a tandem fluorescently tagged LC3 (mCherry/GFP). Upon autophagosome fusion with the lysosome, acidification quenches GFP, but not mCherry. The percent mCherry-positive and GFP-negative (mCherry+/GFP-) cells is a functional autophagy indicator. In PEO1 and OVCAR8 cultured in suspension, there was an average increase of 6.8% and 15.4% mCherry+/GFP- cells compared with adherent cells, respectively (Figures S4E and S4F). Although OVCAR4 adherent cells had a high basal level of mCherry+/GFP- cells (57.4%), suspension culture actually reduced the frequency of mCherry+/GFP- cells by 9.5%, suggesting that, although autophagy is differentially regulated in suspension culture, there are cell-line-dependent effects that require further investigation.

Gene Set Name	# Genes in Gene Set (K)	# Genes in Overlap (k)	k/K	p Value	FDR Q-Value
KEGG					
Pathways in cancer	328	8	2.4%	8.79×10^{-7}	1.63×10^{-4}
Dorsoventral axis formation	25	3	12.0%	2.50×10^{-5}	2.32×10^{-3}
TGF beta signaling pathway	86	4	4.7%	4.56×10^{-5}	2.83×10^{-3}
Taste transduction	52	3	5.8%	2.30×10^{-4}	1.01×10^{-2}
Basal cell carcinoma	55	3	5.5%	2.71×10^{-4}	1.01×10^{-2}
P53 signaling pathway	69	3	4.4%	5.29×10^{-4}	1.53×10^{-2}
Melanoma	71	3	4.2%	5.75×10^{-4}	1.53×10^{-2}
Calcium signaling pathway	178	4	2.3%	7.40×10^{-4}	1.72×10^{-2}
GO Biological Processes					
Circulatory system development	788	19	2.4%	1.75×10^{-14}	7.76×10^{-11}
Regulation of multicellular organismal development	1,672	22	1.3%	2.11×10^{-11}	3.37×10^{-8}
Regulation of cellular component movement	771	16	2.1%	2.28×10^{-11}	3.37×10^{-8}
Positive regulation of developmental process	1,142	18	1.6%	1.02×10^{-10}	1.13×10^{-7}
Regulation of cell differentiation	1,492	20	1.3%	1.42×10^{-10}	1.26×10^{-7}
Tissue development	1,518	20	1.3%	1.92×10^{-10}	1.42×10^{-7}
Epithelium development	945	16	1.7%	4.43×10^{-10}	2.81×10^{-7}
Anatomical structure formation involved in morphogenesis	957	16	1.7%	5.31×10^{-10}	2.93×10^{-7}
Regulation of transport	1,804	21	1.2%	5.95×10^{-10}	2.93×10^{-7}
Blood vessel morphogenesis	364	11	3.0%	7.66×10^{-10}	3.31×10^{-7}
GO Molecular Function					
Receptor binding	1,476	19	1.3%	8.53×10^{-10}	7.68×10^{-7}
Receptor activity	1,649	17	1.0%	1.79×10^{-7}	8.05×10^{-5}
Transporter activity	1,276	14	1.1%	1.17×10^{-6}	3.52×10^{-4}
S100 protein binding	13	3	23.1%	3.17×10^{-6}	6.27×10^{-4}
Kinase activity	842	11	1.3%	3.48×10^{-6}	6.27×10^{-4}
Metal ion transmembrane transporter activity	417	8	1.9%	5.18×10^{-6}	7.18×10^{-4}
Cation channel activity	298	7	2.4%	5.58×10^{-6}	7.18×10^{-4}
Gated channel activity	325	7	2.2%	9.80×10^{-6}	1.10×10^{-3}
Protein kinase activity	640	9	1.4%	1.58×10^{-5}	1.38×10^{-3}
Transferase activity transferring phosphorus containing groups	992	11	1.1%	1.61×10^{-5}	1.38×10^{-3}

Table 3. Pathway Analysis of Significant Genes Common between CRISPR/Cas9 Screen and RNA-Sequencing
Related to Figure 3.

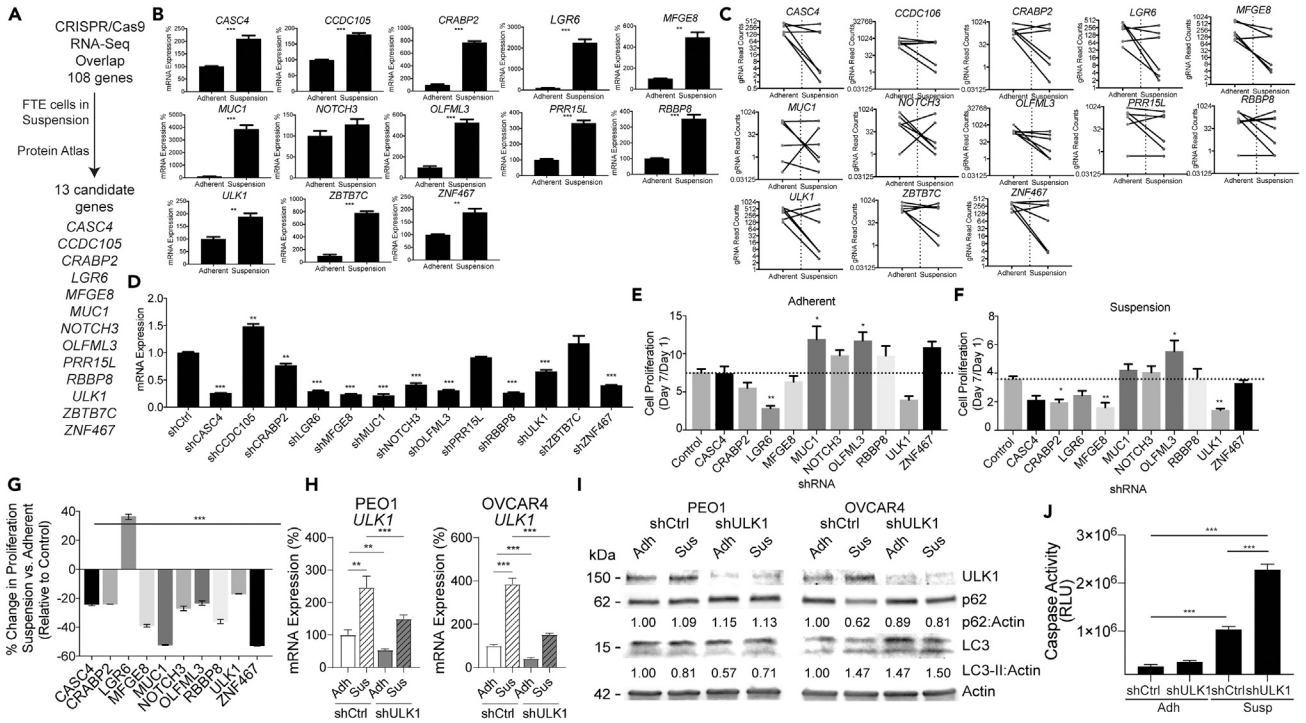


Figure 4. Validation of CRISPR/Cas9 and RNA-seq in HGSOC Cells Reveals an Autophagy Effector

(A) Cross-referencing 108 genes with Protein Atlas and a publicly available dataset examining FTE grown in suspension (GEO: GSE51220). Thirteen genes were selected that are predominantly expressed in ovarian cancer and were significantly changed in FTE cells grown in suspension.

(B) PEO1 cells were grown in adherent and suspension settings for 7 days. RNA was extracted from cells and used for RT-qPCR against indicated genes. Internal control = 18S. Statistical test = two-sided unpaired t test.

(C) All target gRNA counts (y axis) for each of the 13 selected genes in adherent and suspension. Connecting line demonstrate the direction of abundance between adherent and suspension.

(D) Control shRNA and pooled shRNA against the 13 selected genes were transduced into PEO1 cells. RNA was extracted and used for RT-qPCR against indicated gene. 18S = internal control. Statistical test = ANOVA.

(E) shControl and pooled shRNA cells were cultured in adherent conditions for 1 and 7 days. On day 1 and 7 a CyQuant assay examined double-stranded DNA content as a surrogate for cell number. Intensity of CyQuant at Day 7/Day 1 graphed.

(F) Same as (E), but examined cells grown in suspension settings.

(G) Percent change between Adherent and Suspension growth shown in (E) and (F).

(H) shCtrl and shULK1 PEO1 and OVCAR4 cells grown in adherent (Adh) or suspension (Sus) for 48 h. RNA was extracted from cells and used for RT-qPCR against *ULK1*. Internal control = 18S. Statistical test = two-sided unpaired t test.

(I) Same as H, collected protein and immunoblotted against ULK1, p62, and LC3-II. Loading control = Actin. Values underneath blots are densitometry analysis of p62 (top) and LC3-II (bottom) expression normalized to Actin and shCtrl Adh.

(J) OVCAR4 shCtrl and shULK1 cells cultured in adherent (Adh) and suspension (Sus) culture for 48 h. Caspase activity was measured with Caspase-Glo assay. Assays in panels E-G performed in quintuplicate in at least two independent experiments. Statistical test = ANOVA.

*p < 0.05, **p < 0.01, ***p < 0.001. Error bars = S.E.M. See also Figure S4.

We next evaluated ULK1-dependent autophagy by evaluating expression of ULK1, sequestosome 1 (SQSTM1/p62) depletion, and accumulation of lipidated microtubule-associated protein light chain 3 (LC3-II). To assess the role of ULK1 we utilized shULK1 PEO1, OVCAR4, and OVCAR8 cells cultured in suspension. We confirmed the loss of ULK1 protein expression in the three cell lines (Figure S4G). In shCtrl PEO1, OVCAR4, and OVCAR8, both ULK1 mRNA and protein expression were elevated upon suspension culture (Figures 4H–4I and S4H). In shCtrl and shULK1 PEO1 cells cultured in suspension, p62 and LC3 expression remained mostly unchanged (Figure 4I). In contrast, shCtrl OVCAR4 and OVCAR8 suspension cells had depletion of p62 and loss of ULK1 attenuated p62 depletion (Figures 4I and S4F). Furthermore, ULK1 knockdown enhanced forced suspension-induced apoptosis measured via caspase activity (Figure 4J). ULK1 and ULK2 are functionally redundant in the initiation of the pro-survival autophagic response; ULK2 was not identified in either the CRISPR/Cas9 or RNA-seq analysis. Also, ULK1 knockdown in PEO1, OVCAR8, and OVCAR4 cell lines did not promote a *ULK2* compensatory response (Figure S4J). Taken

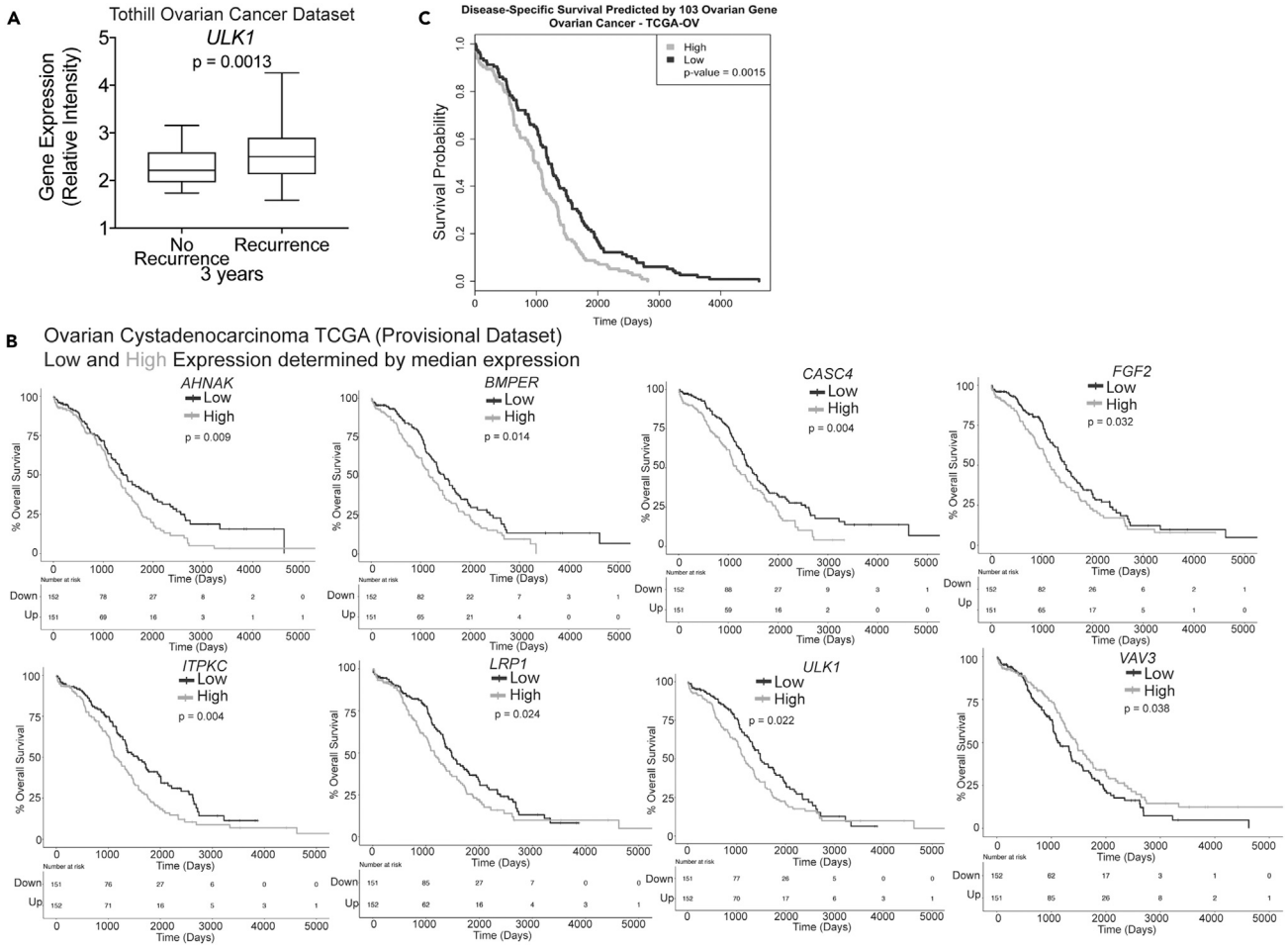


Figure 5. ULK1 Predicts HGSOC Recurrence and Survival and the 108 Gene Signature Predicts Overall Survival

(A) Examination of *ULK1* expression in primary ovarian adenocarcinoma that had no recurrence (n = 23) or recurrence (n = 96) after 3 years. Statistical test = two-sided unpaired t test. Error bars = S.E.M.

(B) A median expression was determined from each indicated gene to distinguish patient tumors with high expression (High, gray line) versus low expression (Low, dark line). KM curves were generated. TCGA (Ovarian cancer, Cancer Genome Atlas Research Network, 2011) dataset was used. Statistical test = Wilcoxon rank sum.

(C) For the TCGA Ovarian Cystadenocarcinoma dataset, 103 genes were mapped to their associated probe set or if the reference dataset was a list of genes, then expression data were pulled out based on matching gene names. Of the candidate genes, there was a varying number of probe sets present on all array platforms. Number of probe sets used indicated above KM curves. For each dataset, modeling survival and generating a KM curve on the candidate gene signature score. The dichotomous description of gene signature score (high or low gene signature score) was assigned. p Values were taken from the log likelihood statistic from the Cox proportional hazard models. For verification, we permuted a subset of random expression and random outcome (time, vital status) values, and broke the relationship between expression and outcome. This was done 1,000 times, and for each permuted dataset we modeled survival as described for the original analysis and generated a distribution of log likelihood statistics. Note: not all genes were identified in each dataset.

together, suspension culture promotes autophagy and ULK1 is upregulated upon forced suspension and contributes to cell survival potentially by promoting an autophagic response.

Given anoikis resistance and dissemination are related to metastasis and a worse prognosis, we determined whether any of the 108 genes, individually or combined could predict survival. As an example, we examined the relationship between *ULK1* expression in primary ovarian adenocarcinoma samples and recurrence at 3 years (No recurrence, n = 23 and Recurrence, n = 96) and found that increased ULK1 expression significantly correlated with recurrence (Figure 5A). We also cross-referenced the individual 108 genes to The Cancer Genome Atlas for ovarian serous cystadenocarcinoma (TCGA, Nature) to determine if mRNA expression correlated to overall survival (Table S6, Column P). "High" and "Low" expression was determined by the median *Z* score. The expression of eight genes correlated with poor overall survival (Figure 5B)

(2011). We developed a gene signature by combining the 108 genes and examined the ovarian serous cystadenocarcinoma (TCGA, Nature) dataset and found that high expression of the top 108 genes significantly ($p = 0.0015$) predicted a worse overall survival (Figure 5C). One caveat is the risk of overfitting the model due to the high number of genes in the candidate list. Therefore, we tested whether our 108 genes would perform better at predicting survival than 108 random genes. We randomly selected genes to serve as permuted gene signatures and used these random genes to evaluate survival. Our 108 gene signature performs significantly better than the permuted models. Taken together, in ovarian cancer we confirmed that the genes identified significantly correlated to ovarian cancer clinical outcomes including metastasis, recurrence, and survival.

Looking beyond Ovarian Cancer

Anoikis escape is required for metastasis in most carcinomas, meaning they resist programmed cell death upon detachment from the ECM. The genes identified in this study could potentially contribute to our understanding of disease progression for multiple carcinomas. The 108 gene signature developed above and the random gene signature were tested against TCGA datasets for a variety of epithelial-derived cancers. Owing to the filtering step, there was not a static number of genes used in every analysis. For most datasets not all 108 genes were retained, but for most datasets at least 100 of the 108 genes were retained and used in the respective analysis. Except for colorectal cancer, our 108 gene set significantly predicted survival better than a random 108 genes (Table S7). All of the Kaplan-Meier (KM) curves show good separation of survival based on the gene signature scores (survival estimates for high scores are in gray and low scores are in black), except the curve for TCGA-COAD-colorectal cancer, which shows curve intersections (Figure 6). Overall, the 108 genes identified through the genome-wide approaches possibly playing a role in HGSOC progression and their expression predicts survival in a variety of carcinomas.

DISCUSSION

Up to 80% of HGSOC is diagnosed at advanced stage and is characterized by extensive peritoneal metastases and development of ascites. HGSOC cells do not undergo a classical metastatic program mainly because of the disease etiology and progression. Most HGSOC are derived from transformed fallopian tube epithelial (FTE) cells on the fallopian tube fimbriae. Transformed FTE form STIC lesions that are histologically characterized by a mutated p53 signature. Completely independent of vasculature or lymphatic invasion, malignant cells within STIC lesions will detach from the ECM, exfoliate into the peritoneum, escape anoikis, and form distant disease. In this report, a combination of genome-wide approaches (CRISPR/Cas9 screen and RNA-seq) in conjunction with non-targeted metabolomics were utilized to evaluate the anchorage-independent transcriptional reprogramming HGSOC cells undergo to escape anoikis and exhibit anchorage independence. Each of the –omic approaches alone provides sufficient biological insight, and there is a significant amount of information gained from each technique individually. However, integration of all of the datasets provides a deeper and more comprehensive understanding of the biology. We identified both known and novel effectors of anoikis and discovered that these effectors predicted overall survival of patients with a variety of carcinomas.

The loss of ECM attachment activates and represses both inside-out (i.e., activation of ligand binding) and outside-in (i.e., ligand binding to a receptor) signaling. NOTCH, TGFβ, and ERBB signaling are well-established pathways that drive anoikis resistance. The CRISPR/Cas9 screen and RNA-seq analyses detected NOTCH (*NOTCH1/3*), TGFβ (*LTBP1/THBS1*), and ERBB (ERBB3/4) signaling pathways, which highlights the strength and confidence of these approaches. NOTCH3 is altered (amplified/overexpressed) in 17% of HGSOC cases, and NOTCH3 alterations correlated to poor overall survival (Hu et al., 2014). TGFβ signaling is similarly linked to anoikis resistance through several mechanisms including promoting an epithelial-to-mesenchymal transition, activation of Akt pathway, and increased SMAD-dependent transcriptional activation (Cieply et al., 2012; Horowitz et al., 2007; Munoz et al., 2008). Latent Transforming Growth Factor β Binding Protein 1 (LTBP1) is a latent ligand for the TGFβ receptor, and upon Thrombospondin-1 (*THBS1*)-mediated cleavage it promotes Akt and Erk activation (reviewed in Xu et al., 2012). Notably, *THBS1* was also a top hit in our dataset; however, in suspended cells the *THBS1* transcript was significantly downregulated and THBS1 gRNAs were depleted suggesting a regulatory role in anoikis. We observed that *ERBB3* and *ERBB4* receptor tyrosine kinases were upregulated in cells grown under forced suspension. ERBB3 is amplified or overexpressed in greater than 50% of HGSOC cases (Cerami et al., 2012; Gao et al., 2013). Pardeep et al. reported that ERBB3 is important for HGSOC dissemination to the omentum and ERBB3 knockdown reduced tumor burden. In contrast, *in vitro* knockdown of

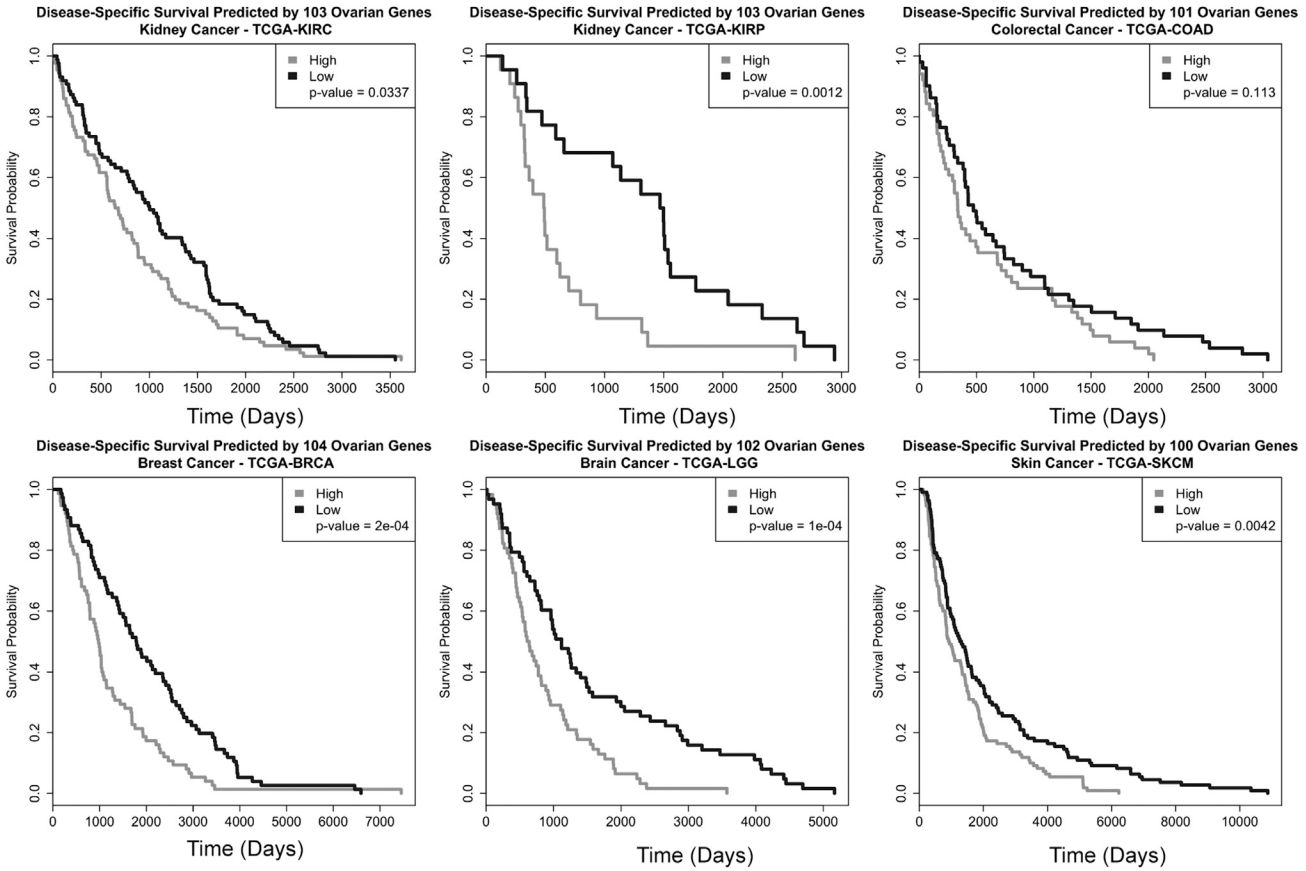


Figure 6. 108 Gene Signature Predicts Overall Survival in Several Epithelial-Derived Cancers

For the TCGA datasets, 108 gene expression data were pulled out based on matching gene names in the hg38 annotation. For each dataset, modeling survival and generating a KM curve on the candidate gene signature score. The dichotomous description of gene signature score (high or low gene signature score) was assigned. p Values were taken from the log likelihood statistic from the Cox proportional hazard models. For verification, we permuted a subset of random expression and random outcome (time, vital status) values and broke the relationship between expression and outcome. This was done 1,000 times, and for each permuted dataset we modeled survival as described for the original analysis and generated a distribution of log likelihood statistics. Note: not all genes were identified in each dataset and the number of genes used to generate KM curves indicated above graphs.

ERBB3 failed to inhibit HGSOC cell proliferation suggesting a regulatory role of the tumor microenvironment or a context-dependent function (Pradeep et al., 2014). The role of ERRB4 in HGSOC is complex. ERRB4 is expressed in 89%–96% of HGSOC tumors, is associated with chemotherapy refractory disease, and has at least three isoforms that are detectable in multiple cellular compartments (Davies et al., 2014; Gilmour et al., 2001). In PEO1 cells, targeting ERRB4 unexpectedly stimulated cell proliferation (Gilmour et al., 2001), highlighting that both ERBB3 and ERBB4 regulate proliferation and dissemination in a context-dependent manner. Our findings are consistent with previous reports that NOTCH, TGFβ, and ERBB signaling are important regulators of anoikis.

Another top hit, Unc-51 like autophagy activating kinase 1 (*ULK1*) is a serine/threonine kinase that under nutrient deprivation promotes autophagy in an AMP-activated protein kinase (AMPK)-dependent fashion (Egan et al., 2015). *ULK1* is expressed in ~40% of HGSOC and is correlated with progressive disease (Cerami et al., 2012; Gao et al., 2013). Consistently, we found *ULK1* expression predicts HGSOC recurrence and overall survival. SBI-0206965 is a small molecule ULK1 inhibitor that, in models of lung and renal clear cell carcinoma, showed anti-cancer effects through inhibition of autophagy and the pentose phosphate pathway (Egan et al., 2015; Lu et al., 2018). In the HGSOC cell lines, forced suspension elevated ULK1 expression and knockdown of ULK1 inhibited cell viability. Notably, forced suspension induced autophagy in two of three cell lines, suggesting an autophagy-independent ULK1 function. For instance, ULK1 is key for stress/metabolic-induced clearance of damaged mitochondria (Kundu et al., 2008). Also, in adipocytes

ULK1 functions to regulate FA oxidation and FA metabolism (Ro et al., 2013). Identification of ULK1 highlights the relationship between autophagy, anoikis, and metabolism.

In light of the metabolomics data demonstrating accumulation of PUFAs in suspension cells, NOTCH, TGFβ, ERBB, and ULK1 signaling have all been linked to increased FA metabolism. In cardiac endothelial cells, NOTCH signaling is an important regulator for FA transport and angiogenesis (Jabs et al., 2018). In hepatocellular carcinoma, TGFβ signaling is associated with increased FA oxidation and increased expression of Peroxisome proliferator-activated receptor gamma, a regulator of FA and glucose metabolism (Soukupova et al., 2017). ERBB signaling contributes to FA synthase by promoting increased expression of *FASN*, a known regulator of HGSOC dissemination (Grunt et al., 2009; Jiang et al., 2014). Loss of ULK1 in adipocytes reduces FA β-oxidation (Ro et al., 2013). The NOTCH, TGFβ, ERBB signaling pathways were highly enriched in our studies, suggesting these pathways are promoting ovarian cancer dissemination in part through promoting FA metabolism. In both ovarian and colon cancer, inhibition of a critical mitochondrial FA transporter, carnitine palmityltransferase I (CPT1), significantly promoted anchorage-independent cell death (Shao et al., 2016; Wang et al., 2018). Clinically applicable drugs (e.g., Etomoxir) have been developed to inhibit FA metabolism and CPT1 for non-oncogenic indications, suggesting that repurposing these drugs might a useful way to exploit a metabolic vulnerability to reduce HGSOC dissemination.

Two of the top CRISPR/Cas9 screen hits, *ACADVL* and *ECHDC2*, are associated with long-chain and very-long-chain FA metabolism and biosynthesis, respectively. Seemingly, these enzymes function on opposite ends of FA biology. Upon knock down of *ACADVL* or *ECHDC2* cells, followed by metabolomics analysis, the suspension-induced PUFA enrichment was significantly attenuated. Similar to most cellular process, FA metabolism maintains energy and signaling equilibrium within cells. In the CRISPR/Cas9 screen, we expect that the loss of *ACADVL* or *ECHDC2* was a mutually exclusive event. In suspension culture, ACADVL or ECHDC2 potentially regulates this equilibrium and loss of these effectors disrupts the equilibrium, exacerbates cellular stress, and reduces cell viability.

In conclusion, we uncovered novel regulators of HGSOC growth in suspension, and potentially, anoikis escape, through a CRISPR/Cas9 gene knockout screen, global metabolomics, and RNA-seq approaches. This project is unique in its use of new, unbiased technology to identify drivers of a critical aspect of ovarian cancer dissemination. We confirmed our top hits in a secondary cell line model and extensively cross-referenced them through several comprehensive and complex HGSOC datasets. The data presented here provide a more complete understanding of pathways that facilitate HGSOC dissemination and ovarian cancer progression and will stimulate development of novel therapeutics.

Limitations of the Study

Most of our primary analyses were performed in PEO1 cells (*TP53*-mutant and *BRCA2*-mutant). We performed validations in several secondary HGSOC cell lines with differing mutational backgrounds, including OVCAR4 (*TP53*-mutant, *BRCA1/2*-wild-type), OVCAR8, and OVARY1847 (both *TP53*-mutant, *BRCA1/2*-wild-type, *ERBB2*-mutant, and *KRAS*-mutant). However, we cannot make predictions for every scenario, as certain mutations that we have not examined may result in different behavior in suspension. For patients, their individual mutational background may significantly affect mechanisms of anoikis resistance. Cross-referencing our gene lists with publicly available ovarian cancer datasets gives us confidence that our findings have clinical importance, but new targets will need to be examined *in vivo* before ultimate significance can be determined. This is especially true of immunocompetent animal models and human patients, in which transformed cells must not only survive in suspension, but must also evade immune surveillance within the peritoneal cavity. We cannot make predictions for immune evasion based only on the *in vitro* data of the current study.

METHODS

All methods can be found in the accompanying Transparent Methods supplemental file.

SUPPLEMENTAL INFORMATION

Supplemental Information can be found online at https://doi.org/10.1016/j.isci.2019.07.049.

ACKNOWLEDGMENTS

We would like to acknowledge Dr. Andrew P. Bradford and Alexandra McMellen for critical reading of this manuscript. This work was supported by the National Institutes of Health (B.G.B., R00CA194318; J.M.E., R01CA117907 and R01GM120109), the Department of Defense OCRP (B.G.B., OC170228), as well as the American Cancer Society (L.J.W., ACS-IRG and B.T.S., ACS-IRG, 16-184-56), the University of Colorado Department of Obstetrics and Gynecology Academic Enrichment Fund (AEF), RNA Biosciences Initiative (J.K.R.), and the University of Colorado Cancer Center Support Grant (P30CA046934).

AUTHOR CONTRIBUTIONS

L.J.W., Z.L.W., and B.G.B. conceived of the project and experiments. L.J.W., Z.L.W., T.M.Y., M.J., S.W.B., and B.G.B. designed and performed experiments. L.J.W., Z.L.W., L.Q., T.M.Y., B.T.S., K.D.S., S.K., V.F.-R., H.S., L.A.V., C.M.C., H.K., J.M.E., J.K.R., and B.G.B. synthesized and analyzed data and aided in interpretation. L.J.W., Z.L.W., and B.G.B. wrote the manuscript. All authors read and revised the manuscript and have read and approved of this version of the manuscript.

DECLARATION OF INTERESTS

The authors declare no competing financial interests.

Received: March 12, 2019
Revised: June 24, 2019
Accepted: July 30, 2019
Published: September 27, 2019

REFERENCES

Bahnson, B.J., Anderson, V.E., and Petsko, G.A. (2002). Structural mechanism of enoyl-CoA hydratase: three atoms from a single water are added in either an E1cb stepwise or concerted fashion. Biochemistry *41*, 2621–2629.

Berek, J.S., and Hacker, N.F. (2015). Berek & Hacker's Gynecologic Oncology (Wolters Kluwer Health/Lippincott Williams & Wilkins).

Bian, Y., Yu, Y., Wang, S., and Li, L. (2015). Up-regulation of fatty acid synthase induced by EGFR/ERK activation promotes tumor growth in pancreatic cancer. Biochem. Biophys. Res. Commun. *463*, 612–617.

Brown, C.W., Brodsky, A.S., and Freiman, R.N. (2015). Notch3 overexpression promotes anoikis resistance in epithelial ovarian cancer via upregulation of COL4A2. Mol. Cancer Res. *13*, 78–85.

Cancer Genome Atlas Research Network (2011). Integrated genomic analyses of ovarian carcinoma. Nature *474*, 609–615.

Cerami, E., Gao, J., Dogrusoz, U., Gross, B.E., Sumer, S.O., Aksoy, B.A., Jacobsen, A., Byrne, C.J., Heuer, M.L., Larsson, E., et al. (2012). The cBio cancer genomics portal: an open platform for exploring multidimensional cancer genomics data. Cancer Discov. *2*, 401–404.

Cieply, B., Riley, P.T., Pifer, P.M., Widmeyer, J., Addison, J.B., Ivanov, A.V., Denvir, J., and Frisch, S.M. (2012). Suppression of the epithelial-mesenchymal transition by Grainyhead-like-2. Cancer Res. *72*, 2440–2453.

Davies, S., Holmes, A., Lomo, L., Steinkamp, M.P., Kang, H., Muller, C.Y., and Wilson, B.S. (2014). High incidence of ErbB3, ErbB4, and MET expression in ovarian cancer. Int. J. Gynecol. Pathol. *33*, 402–410.

Van Der Steen, S., Bulten, J., Van De Vijver, K.K., Van Kuppevelt, T.H., and Massuger, L. (2017). Changes in the extracellular matrix are associated with the development of serous tubal intraepithelial carcinoma into high-grade serous Carcinoma. Int. J. Gynecol. Cancer *27*, 1072–1081.

Egan, D.F., Chun, M.G., Vamos, M., Zou, H., Rong, J., Miller, C.J., Lou, H.J., Raveendra-Panickar, D., Yang, C.C., Sheffler, D.J., et al. (2015). Small molecule inhibition of the autophagy kinase ULK1 and identification of ULK1 substrates. Mol. Cell *59*, 285–297.

Gao, J., Aksoy, B.A., Dogrusoz, U., Dresdner, G., Gross, B., Sumer, S.O., Sun, Y., Jacobsen, A., Sinha, R., Larsson, E., et al. (2013). Integrative analysis of complex cancer genomics and clinical profiles using the cBioPortal. Sci. Signal. *6*, pl1.

Gao, Q., Yang, Z., Xu, S., Li, X., Yang, X., Jin, P., Liu, Y., Zhou, X., Zhang, T., Gong, C., et al. (2019). Heterotypic CAF-tumor spheroids promote early peritoneal metastasis of ovarian cancer. J. Exp. Med. *216*, 688–703.

Gilmour, L.M., Macleod, K.G., Mccaig, A., Gullick, W.J., Smyth, J.F., and Langdon, S.P. (2001). Expression of erbB-4/HER-4 growth factor receptor isoforms in ovarian cancer. Cancer Res. *61*, 2169–2176.

Grunt, T.W., Wagner, R., Grusch, M., Berger, W., Singer, C.F., Marian, B., Zielinski, C.C., and Lupu, R. (2009). Interaction between fatty acid synthase- and ErbB-systems in ovarian cancer cells. Biochem. Biophys. Res. Commun. *385*, 454–459.

Horowitz, J.C., Rogers, D.S., Sharma, V., Vittal, R., White, E.S., Cui, Z., and Thannickal, V.J. (2007). Combinatorial activation of FAK and AKT by transforming growth factor-beta1 confers an anoikis-resistant phenotype to myofibroblasts. Cell Signal. *19*, 761–771.

Hu, W., Liu, T., Ivan, C., Sun, Y., Huang, J., Mangala, L.S., Miyake, T., Dalton, H.J., Pradeep, S., Rupaimoole, R., et al. (2014). Notch3 pathway alterations in ovarian cancer. Cancer Res. *74*, 3282–3293.

Jabs, M., Rose, A.J., Lehmann, L.H., Taylor, J., Moll, I., Sijmonsma, T.P., Herberich, S.E., Sauer, S.W., Poschet, G., Federico, G., et al. (2018). Inhibition of endothelial notch signaling impairs fatty acid transport and leads to metabolic and vascular remodeling of the adult heart. Circulation *137*, 2592–2608.

Jayson, G.C., Kohn, E.C., Kitchener, H.C., and Ledermann, J.A. (2014). Ovarian cancer. Lancet *384*, 1376–1388.

Jiang, L., Wang, H., Li, J., Fang, X., Pan, H., Yuan, X., and Zhang, P. (2014). Up-regulated FASN expression promotes transcoelomic metastasis of ovarian cancer cell through epithelial-mesenchymal transition. Int. J. Mol. Sci. *15*, 11539–11554.

Kim, S., Kim, B., and Song, Y.S. (2016). Ascites modulates cancer cell behavior, contributing to tumor heterogeneity in ovarian cancer. Cancer Sci. *107*, 1173–1178.

Kundu, M., Lindsten, T., Yang, C.Y., Wu, J., Zhao, F., Zhang, J., Selak, M.A., Ney, P.A., and Thompson, C.B. (2008). Ulk1 plays a critical role in the autophagic clearance of mitochondria and ribosomes during reticulocyte maturation. Blood *112*, 1493–1502.

Kurtz, D.M., Rinaldo, P., Rhead, W.J., Tian, L., Millington, D.S., Vockley, J., Hamm, D.A., Brix, A.E., Lindsey, J.R., Pinkert, C.A., et al. (1998). Targeted disruption of mouse long-chain acyl-CoA dehydrogenase gene reveals crucial roles for fatty acid oxidation. Proc. Natl. Acad. Sci. U S A *95*, 15592–15597.

Lawrenson, K., Notaridou, M., Lee, N., Benjamin, E., Jacobs, I.J., Jones, C., and Gayther, S.A. (2013). In vitro three-dimensional modeling of fallopian tube secretory epithelial cells. BMC Cell Biol. *14*, 43.

Lee, Y., Miron, A., Drapkin, R., Nucci, M.R., Medeiros, F., Saleemuddin, A., Garber, J., Birch, C., Mou, H., Gordon, R.W., et al. (2007). A candidate precursor to serous carcinoma that originates in the distal fallopian tube. J. Pathol. *211*, 26–35.

Lengyel, E., Burdette, J.E., Kenny, H.A., Matei, D., Pilrose, J., Haluska, P., Nephew, K.P., Hales, D.B., and Stack, M.S. (2014). Epithelial ovarian cancer experimental models. Oncogene *33*, 3619–3633.

Liu, Y., Metzinger, M.N., Lewellen, K.A., Cripps, S.N., Carey, K.D., Harper, E.I., Shi, Z., Tarwater, L., Grisoli, A., Lee, E., et al. (2015). Obesity contributes to ovarian cancer metastatic success through increased lipogenesis, enhanced vascularity, and decreased infiltration of M1 macrophages. Cancer Res. *75*, 5046–5057.

Lu, J., Zhu, L., Zheng, L.P., Cui, Q., Zhu, H.H., Zhao, H., Shen, Z.J., Dong, H.Y., Chen, S.S., Wu, W.Z., and Tan, J.M. (2018). Overexpression of ULK1 represents a potential diagnostic marker for clear cell renal carcinoma and the Antitumor effects of SBI-0206965. EBioMedicine *34*, 85–93.

Miranda, F., Mannion, D., Liu, S., Zheng, Y., Mangala, L.S., Redondo, C., Herrero-Gonzalez, S., Xu, R., Taylor, C., Chedom, D.F., et al. (2016). Salt-inducible kinase 2 couples ovarian cancer cell metabolism with survival at the adipocyte-rich metastatic niche. Cancer Cell *30*, 273–289.

Mizushima, N. (2010). The role of the Atg1/ULK1 complex in autophagy regulation. Curr. Opin. Cell Biol. *22*, 132–139.

Munoz, N.M., Baek, J.Y., and Grady, W.M. (2008). TGF-beta has paradoxical and context dependent effects on proliferation and anoikis in human colorectal cancer cell lines. Growth Factors *26*, 254–262.

Piek, J.M., Van Diest, P.J., Zweemer, R.P., Jansen, J.W., Poort-Keesom, R.J., Menko, F.H., Gille, J.J., Jongsma, A.P., Pals, G., et al. (2001). Dysplastic changes in prophylactically removed Fallopian tubes of women predisposed to developing ovarian cancer. J. Pathol. *195*, 451–456.

Pradeep, S., Kim, S.W., Wu, S.Y., Nishimura, M., Chaluvally-Raghavan, P., Miyake, T., Pecot, C.V., Kim, S.J., Choi, H.J., Bischoff, F.Z., et al. (2014). Hematogenous metastasis of ovarian cancer: rethinking mode of spread. Cancer Cell *26*, 77–91.

Ro, S.H., Jung, C.H., Hahn, W.S., Xu, X., Kim, Y.M., Yun, Y.S., Park, J.M., Kim, K.H., Seo, M., Ha, T.Y., et al. (2013). Distinct functions of Ulk1 and Ulk2 in the regulation of lipid metabolism in adipocytes. Autophagy *9*, 2103–2114.

Shao, H., Mohamed, E.M., Xu, G.G., Waters, M., Jing, K., Ma, Y., Zhang, Y., Spiegel, S., Idowu, M.O., and Fang, X. (2016). Carnitine palmitoyltransferase 1A functions to repress FoxO transcription factors to allow cell cycle progression in ovarian cancer. Oncotarget *7*, 3832–3846.

Soukupova, J., Malfettone, A., Hyrossova, P., Hernandez-Alvarez, M.I., Penuelas-Haro, I., Bertran, E., Junza, A., Capellades, J., Giannelli, G., Yanes, O., et al. (2017). Role of the transforming growth factor-beta in regulating hepatocellular carcinoma oxidative metabolism. Sci. Rep. *7*, 12486.

Szklarczyk, D., Morris, J.H., Cook, H., Kuhn, M., Wyder, S., Simonovic, M., Santos, A., Doncheva, N.T., Roth, A., Bork, P., et al. (2017). The STRING database in 2017: quality-controlled protein-protein association networks, made broadly accessible. Nucleic Acids Res. *45*, D362–D368.

Tone, A.A., Begley, H., Sharma, M., Murphy, J., Rosen, B., Brown, T.J., and Shaw, P.A. (2008). Gene expression profiles of luteal phase fallopian tube epithelium from BRCA mutation carriers resemble high-grade serous carcinoma. Clin. Cancer Res. *14*, 4067–4078.

Toyama, A., Suzuki, A., Shimada, T., Aoki, C., Aoki, Y., Umino, Y., Nakamura, Y., Aoki, D., and Sato, T.A. (2012). Proteomic characterization of ovarian cancers identifying annexin-A4, phosphoserine aminotransferase, cellular retinoic acid-binding protein 2, and serpin B5 as histology-specific biomarkers. Cancer Sci. *103*, 747–755.

Uhlen, M., Oksvold, P., Fagerberg, L., Lundberg, E., Jonasson, K., Forsberg, M., Zwahlen, M., Kampf, C., Wester, K., Hober, S., et al. (2010). Towards a knowledge-based human protein Atlas. Nat. Biotechnol. *28*, 1248–1250.

Uhlen, M., Fagerberg, L., Hallstrom, B.M., Lindskog, C., Oksvold, P., Mardinoglu, A., Sivertsson, A., Kampf, C., Sjostedt, E., Asplund, A., et al. (2015). Proteomics. Tissue-based map of the human proteome. Science *347*, 1260419.

Wang, Y.N., Zeng, Z.L., Lu, J., Wang, Y., Liu, Z.X., He, M.M., Zhao, Q., Wang, Z.X., Li, T., Lu, Y.X., et al. (2018). CPT1A-mediated fatty acid oxidation promotes colorectal cancer cell metastasis by inhibiting anoikis. Oncogene *37*, 6025–6040.

Wheeler, L.J., Watson, Z.L., Qamar, L., Yamamoto, T.M., Post, M.D., Berning, A.A., Spillman, M.A., Behbakht, K., and Bitler, B.G. (2018). CBX2 identified as driver of anoikis escape and dissemination in high grade serous ovarian cancer. Oncogenesis *7*, 92.

Xu, P., Liu, J., and Derynck, R. (2012). Post-translational regulation of TGF-beta receptor and Smad signaling. FEBS Lett. *586*, 1871–1884.

ISCI, Volume *19*

Supplemental Information

Multi-Omic Approaches Identify Metabolic and Autophagy Regulators Important in Ovarian Cancer Dissemination

Lindsay J. Wheeler, Zachary L. Watson, Lubna Qamar, Tomomi M. Yamamoto, Brandon T. Sawyer, Kelly D. Sullivan, Santosh Khanal, Molishree Joshi, Veronique Ferchaud-Roucher, Harry Smith, Lauren A. Vanderlinden, Sky W. Brubaker, Cecilia M. Caino, Hyunmin Kim, Joaquin M. Espinosa, Jennifer K. Richer, and Benjamin G. Bitler

Supplemental Figures and Figure Legends

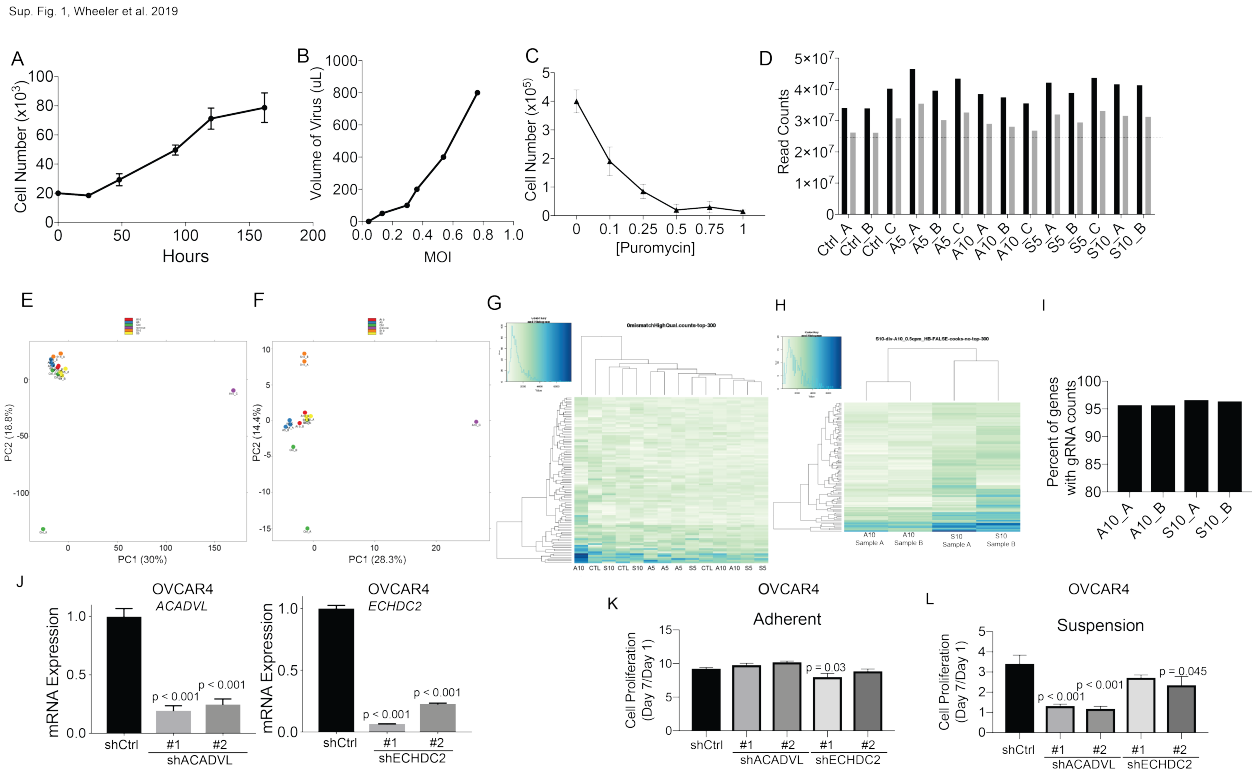


Figure S1. An HGSOC cell line grown in suspension and a CRISPR/Cas9 Screen. (Related to Figure 1) A) PEO1 cells were plated in a low attachment plate (poly-HEMA coated) and grown for 168 hours. **B**) Multiplicity of infection (MOI) of GeCKO library on PEO1 cells. **C**) Puromycin kill curve for PEO1 cells. **D**) Read counts for each sample - black bars = raw count and gray bars = counts of perfect match quality reads. **E**) Principal component analysis of all samples. **F**) Principal component analysis after removing A10_C (purple dot). **G**) Unsupervised hierarchal clustering of top 300gRNA from all samples. **H**) Unsupervised hierarchal clustering of top 300 gRNA comparing adherent day 10 (A and B) with suspension day 10 (A and B). **I)** Percent of genes with at least one gRNA detected in A10 (A and B) and S10 (A and B). **J)** OVCAR4 cells were transduced with shControl (shCtrl) or shACADVL (#1 and #2) or shECHDC2 (#1 and #2). RNA was extracted from cells and used for qRT-PCR against *ACADVL* and *ECHDC2*. Internal control = *18s*. **K)** OVCAR4 shCtrl, shACADVL, and shECDHC2 cells were plated on tissue culture treated plastic (adherent) on day 0. Double strand DNA content was used as a surrogate for cell number and was measured on day 1 and day 7. Y-axis represents the change in cell number from Day 1 to Day 7. **L)** OVCAR4 shCtrl, shACADVL, and shECDHC2 cells were plated in low adherent tissue culture plates (suspension) and double strand DNA content was measured on day 1 and day 7. Y-axis represents the change in cell number from Day 1 to Day 7. Statistical test = ANOVA. Error bars = S.E.M.

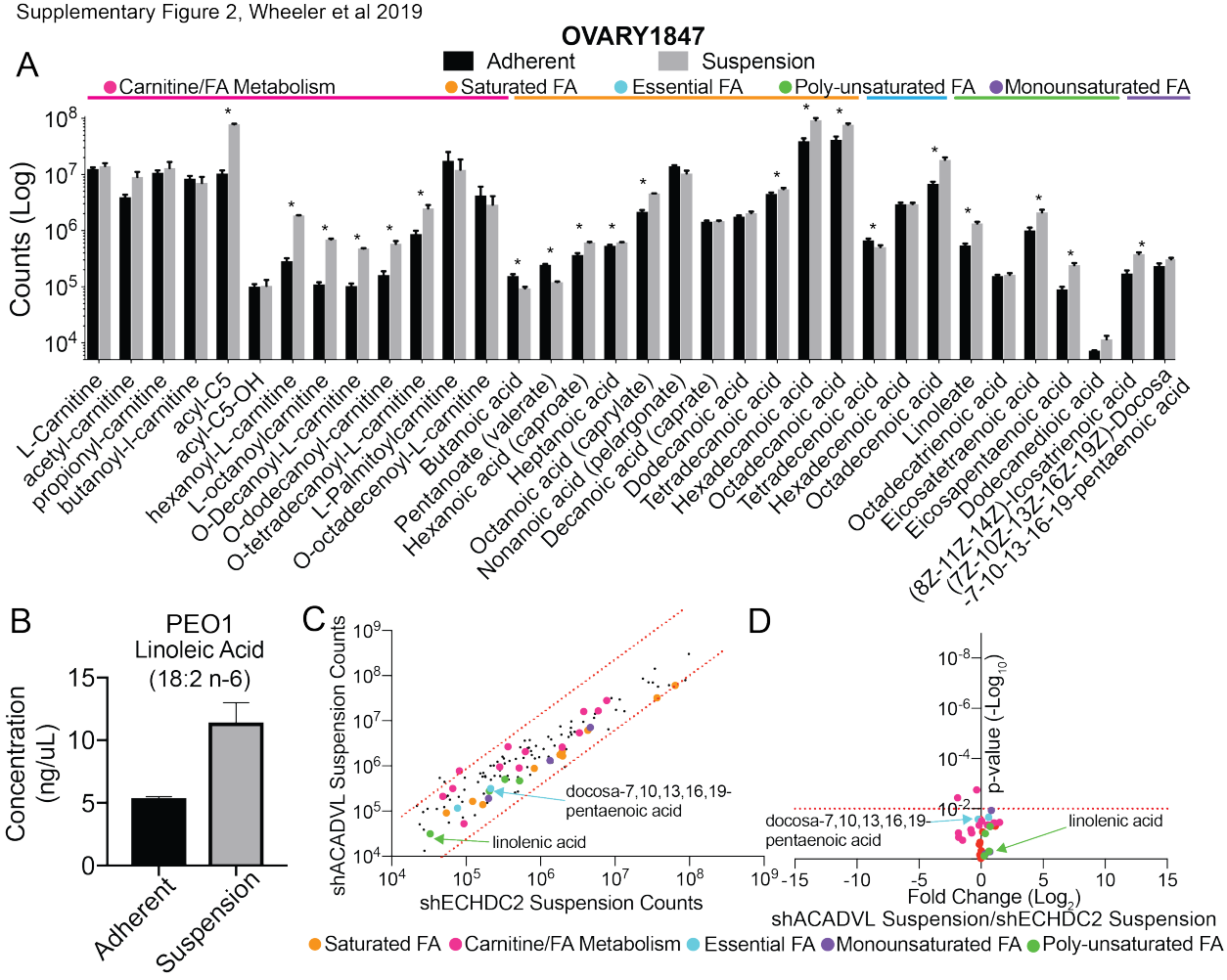


Figure S2. HGSOC cells cultured in suspension are enriched for fatty acids and fatty acid metabolites. (Related to Figure 2) A) HGSOC cells (OVARY1847) were cultured in adherent and suspension cultures for 48 hrs. Cells were collected and used for global non-targeted metabolomics. Fatty acids and fatty acids metabolites are shown for OVARY1847 cells grown in adherent (black bars) or suspension (gray bars) conditions. *p-value < 0.05. **B)** PEO1 cells were grown in adherent and suspension culture for seven days. Cells were collected, fatty acids were extracted, and the extracts were used for mass spec. **C**) Global non-targeted metabolomics analysis of shACADVL PEO1 cells cultured in suspension versus shECHDC2 PEO1 cells cultured in suspension. Metabolite counts graphed as a scatter plot. x-axis – shECHDC2 suspension and y-axis – shACADVL1 suspension. Red dotted line indicated p-value threshold. **D)** Same as C, but scatter plot of log2 fold change – x-axis and p-value -axis. Red dotted line indicates p-value threshold. Error bars = S.E.M.

Supplementary Figure 3, Wheeler et al 2018

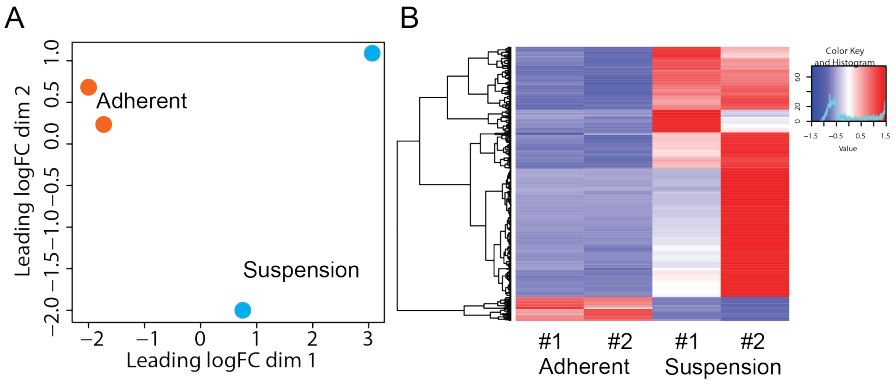


Figure S3. Principal component analysis (A) and hierarchical clustering (B) of RNA-sequencing data. (Related to Figure 3) A) PEO1 cells were grown in adherent or suspension cultures for 10 days. RNA was extracted from cells and utilized for RNA-sequencing. Principal component analysis of replicates for Adherent (red) and Suspension (blue) samples. **B**) Unsupervised hierarchical clustering of 300 top differentially regulated genes ($p<0.0001$).

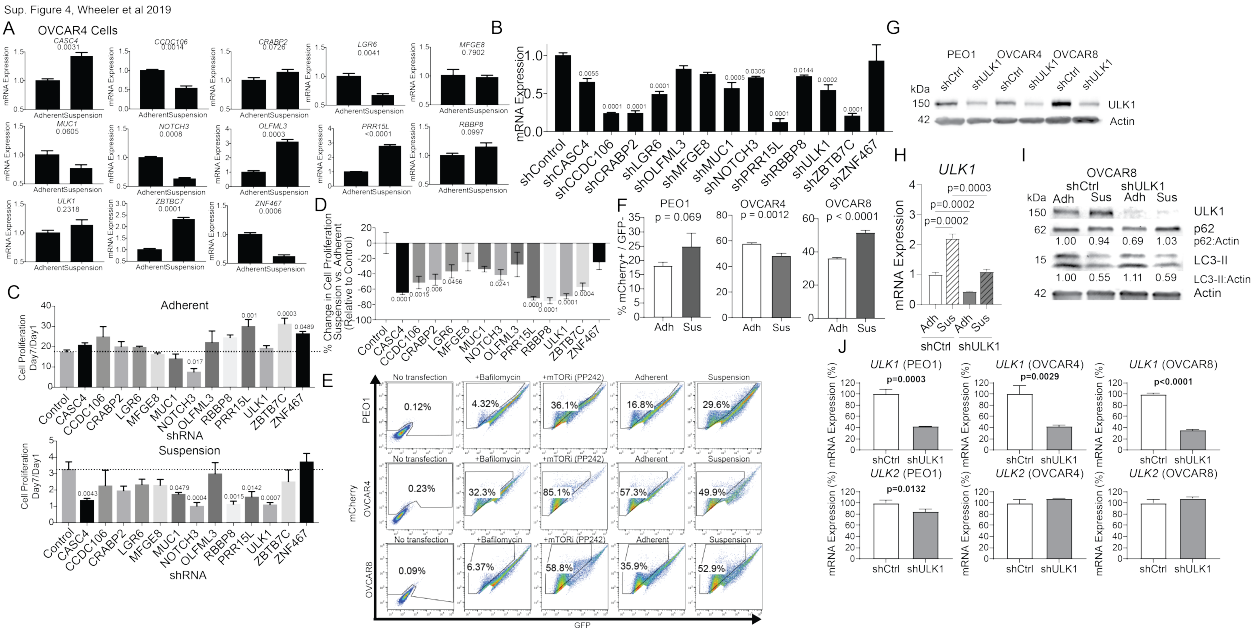


Figure S4. Confirmation of CRISPR/Cas9 and RNA-seq in HGSOC OVCAR4 cells. (Related to Figure 4) A) OVCAR4 cells were grown in adherent and suspension settings for 7 days. RNA was extracted from cells and used for RT-qPCR against indicated genes. 18S = internal control. Statistical test = two-sided unpaired t-test. **B)** Control shRNA and pooled shRNA against the 13 selected genes were transduced into OVCAR4 cells. RNA was extracted and used for RT-qPCR against indicated small hairpin targeted gene. 18S = internal control. Statistical test = ANOVA. **C**) shControl (Control) and pooled shRNA cells were cultured in adherent conditions for 1 and 7 days. On days 1 and 7 a CyQuant assay examined double stranded DNA content as a surrogate for cell number. Intensity of CyQuant at Day 7/Day 1 graphed. **D**) Percent change between Adherent and Suspension growth shown in C. Statistical test = ANOVA. Error bars = S.E.M. **E)** PEO1, OVCAR4, and OVCAR8 cells were transfected with plasmid ptfLC3 encoding a tandem fluorescent mCherry/GFP-tagged LC3. After 24 hrs, cells were seeded into adherent and suspension conditions for 48 hrs, and then analyzed by flow cytometry. Loss of GFP indicates lysosomal fusion with autophagosomes. Representative gating strategy of mCherry positive and GFP negative cells. Non-transfected cells are negative for mCherry and GFP and were gated out in subsequent analyses. Negative control: Transfected cells were treated with 100 nM bafilomycin A1 for 16 hrs. Positive control: Transfected cells were treated with 10 μM mTOR inhibitor (mTORi) PP242 for 16 hrs. **F)** Percentage of cells that are mCherry+/GFP-. Data are plotted as mean. Error bars = S.D. N=3. Statistical test = two-sided t-test. **G)** PEO1, OVCAR4, OVCAR8 cells were transduced with shCtrl or shULK1. Protein was collected and used for immunoblot against ULK1. Loading Control = Actin. **H)** shCtrl and shULK1 OVCAR8 cells cultured adherent (Adh) and suspension (Sus) for 48 hrs. RNA was collected and used for qRT-PCR against *ULK1*. Internal Control = *GAPDH*. Statistical test = two-sided unpaired t-test. Error bars = S.D. **I)** Same as I, but protein was also collected and used for immunoblot against ULK1, p62, and LC3-II. Loading Control = Actin. Values underneath blots are densitometry analysis of p62 (top) and LC3-II (bottom) expression normalized to Actin and shCtrl Adh. **J**) RT-qPCR for *ULK1* and *ULK2* in PEO1, OVCAR4, and OVCAR8 shCtrl and shULK1 cells. Internal control = *GAPDH*. Statistical test = two-sided unpaired t-test. Error bars = S.D.

Transparent Methods

Cell Culture. PEO1, OVCAR4, OVCAR8, and OVARY1847 human high grade serous ovarian cancer cell lines were authenticated using small tandem repeat (STR) analysis (The University of Arizona Genetics Core). HGSOC cells were cultured in RMPI-1640 medium supplemented with 1% penicillin-streptomycin and 10% fetal bovine serum. 293FT cells were cultured in high-glucose DMEM supplemented with 1% penicillin-streptomycin and 10% fetal bovine serum. All cells were maintained in 5% CO_2 at 37 °C and were monthly tested for mycoplasma using LookOut Mycoplasma PCR Detection Kit (Sigma, MP0035). PEO1 cells utilized for the GeCKO screen had been thawed within the previous three weeks.

Immunoblotting and Densitometry of Autophagy Proteins. Cells were lysed and briefly sonicated in RIPA buffer (150 mM NaCl, 1% TritonX-100, 0.5% sodium deoxycholate, 0.1% SDS, 50 mM Tris pH 8.0) supplemented with cOmplete EDTA-free protease inhibitors (Roche #11873580001). Protein was separated by SDS-PAGE and transferred to PVDF membrane using the TransBlot Turbo (BioRad). Membranes were blocked for 1 hour at room temperature in LI-COR Odyssey buffer (LI-COR #927-50000). Primary antibody was incubated overnight at 4 °C in Odyssey buffer. Primary antibodies and concentrations were: rabbit-anti-ULK1 (Cell Signaling #8054, 1:1000), mouse-anti-p62/SQSTM1 (Cell Signaling #88588, 1:1000), mouse-anti-β-actin (Abcam ab6276, 1:10,000), and rabbit-anti-LC3A/B (Cell Signaling #4108, 1:1000). Membranes were washed 3 times for 5 minutes each in TBST (50 mM Tris pH 7.5, 150 mM NaCl, 0.1% Tween-20), then incubated in LI-COR IRDye 800CW secondary antibodies (goat-anti-mouse #925-32210 or goat-anti-rabbit #925-32211) at 1:20,000 dilution in Odyssey buffer for one hour at room temperature. Following an additional 3 washes in TBST, blots were scanned using the LI-COR Odyssey Imaging System. Protein band intensity was quantified using LI-COR Image Studio v4.0 software. LC3-II and p62 were normalized to Actin for each sample, with shCtrl Adherent condition set as 1.00.

Viral Transduction Preparation. PEO1 cells transduced with GeCKO lentivirus were selected with 0.5 μg/mL puromycin. The Functional Genomics Facility (FGF) at the University of Colorado packaged the GeCKO library into lentiviral particles using pΔ8.9 and pCMV-VSV-G packaging vectors. Viral titers were performed on PEO1 cells to determine multiplicity of infection (MOI). Dilutions ranging from 50 to 800 μl of lentivirus in 1mL of media were used to transduce PEO1 cells and incubated for 24 hours. Puromycin selection was performed and the cells were counted at 48 hours when all non-transduced cells had died. The MOI was calculated, and given a goal MOI of 0.5, the optimal dilution of lentivirus was deemed to be 35-40%.

Viral Transduction. GeCKO library lentivirus particles were packaged at the FGF. PEO1 cells were plated on 19 - 15 cm dishes and allowed to recover for 24 hours. Transduction of the GeCKO library was performed at an MOI of 0.5 with polybrene (8 μg/mL). A dish was maintained as a non-transduced control. The transduction reaction incubated for 16 hours. Two 5 million cell aliquots were collected, snap frozen, and stored in -80 °C freezer, as “Post-Transduction Collection.” Cells were selected with puromycin every 24 hours for a total of 72 hours. Puromycin containing media was removed from all plates and cells were allowed to recover for 7 days in the adherent setting with media change and split as needed. Three post-selection samples of 5 million cell aliquots were collected, snap frozen, and stored in -80 °C freezer.

CRISPR/Cas9 Genome-Wide Screen. Following post-selection recovery period, cells were plated on tissue culture dishes treated without (adherent) or with (suspension) poly-HEMA (6 mg/mL). Given findings of slower growth in suspension setting, each adherent dish was plated with 5 million cells, while each suspension dish was plated with 10 million cells. For the adherent dishes, media was changed every 48 hours and cells were split at 90% confluence. For the suspension plates, fresh media was added at the same intervals as the adherent cells. Cells were checked daily for media exhaustion and optimal confluence (<90%). At days 5 and 10 a minimum of 5 million cells was collected for both adherent and suspension conditions. Cell pellets were snap frozen and stored at -80 °C until DNA extraction. DNA extraction was performed using the Quick DNA Mini-Prep protocol (Zymo Research). Nuclease-free water was used for elution and heated to 65 °C to increase yield. Total elution volume was 50 μL. DNA concentration was measured using the NanoDrop.

gRNA Library Preparation. Before initiation of the screen, as part of quality assurance, barcoding and sequencing primers (Table S8) were confirmed to amplify the product of interest. We utilized Q5 polymerase for all PCR (New England BioLabs). As previously described [1], we followed a nested PCR protocol, where the product of PCR1 served as the template for PCR2. To standardize PCR conditions all DNA samples were resuspended to 100 ng/μl. PCR1 was performed in a 60 μl reaction with 1 μg of sample template. PCR1 and 2 were run with the following program: initial 98 °C for 5 min, followed by 98 °C for 30 sec, 60 °C for 30 sec, 72 °C for 30 sec for 15 cycles, and 72 °C for 7 min. Ten microliters of PCR1 was run on gel electrophoresis to confirm product size. In PCR2, the product is 195 base pairs, and the reverse primer included a 16bp barcode. The remaining PCR1 product was used as a starting template for PCR2. A small proportion of samples did not have a 500 base pair band on the initial run. For these samples, the concentration was recalculated using the NanoDrop and purified using the DNA Clean Up kit (Zymo Research). These samples were then run through PCR1 for a second time, and a 500 base pair band was noted on the subsequent gel. All purified PCR products underwent spectrophotometry using the NanoDrop. Each PCR2 product was run on a 2% agarose gel and a band was noted at 200 base pairs. Amplification product was cut out and purified using a Gel Extraction Kit (Qiagen) as per the manufacturer's instructions. The samples were quantified in duplicate using the QuBit (Thermo Scientific).

RNA-sequencing. As previously described [2]. RNA was isolated from PEO1 adherent (n=2) and suspension (n=2) following 7 days of growth using RNeasy columns with on-column DNase digest (Qiagen). RNA quality was confirmed using an Agilent Tapestation and all RNA used for library preparation had a RIN>9. Libraries were created using Illumina TruSEQ stranded mRNA library prep (#RS-122-2102) at the Genomics Core (The University of Colorado). HISAT2 [3] was used for alignment against GRCh37 version of the human genome. Samples were normalized using TPM (Transcripts per Million) measurement and gene expression using the GRCh37 gene annotation was calculated using home-made scripts. The analysis was performed by the Division of Translational Bioinformatics and Cancer Systems Biology at the University of Colorado School of Medicine.

Next Generation Sequencing. During the pre-sequencing quality assurance was performed on an Agilent Tapestation. PCR2 amplicons were sequenced at the Genomics Core (The University of Colorado) or Novogene Corporation. The Genomics Core pooled the libraries for sequencing. Libraries were sequenced on the HiSeq4000 and HiSeq2500 (Illumina). Due to sequence homology between libraries the pooled library sample was spiked with PhiX (15%).

CRISPR/Cas9 Sequencing Analysis. gRNA sequencing and differential gRNA analysis were conducted as previously described [1]. Principal component analysis and hierarchical clustering of the gRNA reads counts found that one Adherent Day 10 sample was different compared to the other collection points (Fig. S1E-G). This sample was removed from our analysis.

Global non-targeted metabolomics. As previously described [4]. PEO1 and OVARY1847 cells were cultured in adherent and suspension for 48 hrs. One million adherent and suspension cells were analyzed. Ultra-high performance liquid chromatography-mass spectrometry metabolomics was performed by University of Colorado School of Medicine Biological Mass Spectrometry Facility.

Reverse Transcription Quantitative Polymerase Chain Reaction (RT-qPCR). RNA was isolated using RNAeasy Mini Kit (Qiagen) according to the manufacturer's protocol. NanoDrop spectrophotometry was performed to confirm the concentration of extracted RNA. RT-qPCR was performed using the Luna Universal One-step Reaction kit (New England BioLabs) on a BioRad CFX96 thermocycler with primers for each of the top genes of interest; 18S rRNA were utilized as internal controls (Table S9).

shRNA Knockdown. As previously described [5]. Gene specific shRNAs were obtained from the University of Colorado Functional Genomics Facility (Table S10). Plasmid isolation was performed using the Plasmid Midi-Prep Kit (Qiagen). Twenty-four hours after seeding, cells were transfected with a total of 12 μg of DNA, including lentiviral packaging plasmids and the shRNA, in addition to 36 μg of polyethyenimine (PEI), for a ratio of 1:3, DNA to PEI. Cells were incubated overnight and transitioned to Dulbecco's Modified Eagle Media (DMEM) the following morning. Forty-eight hours after medium change,

lentivirus was harvested. PEO1 cells were seeded into six-well plates. When cells reached 80% confluence, they were transduced with lentivirus encoding gene-specific shRNAs or a scrambled shRNA control. A control well was maintained without virus to confirm puromycin selection. A 48-hour puromycin selection was performed immediately following transduction. After medium change cells were allowed to recover then subjected to functional assays.

CyQuant Viability Assay. HGSOC cells were seeded in a 96-well plate and treated for 72 hours. Cells were incubated with CyQuant Direct (Thermo Fisher, Cat # 35011) for 2 hours. Fluorescence was measured on a Molecular Devices SpectraMax M2 microplate reader. Excitation = 508nm/Emission = 527nm.

Autophagy Assay. PEO1 or OVCAR8 cells were transfected using a 3:1 ratio of FuGENE 6 transfection reagent (Promega) and plasmid ptfLC3 (Addgene plasmid #21074, [6]). ptfLC3 encodes a tandem fluorescent mCherry/GFP-tagged LC3. After 24 h, cells were seeded into adherent and suspension conditions, then incubated for 48 h prior to collection for flow cytometry. For negative control, cells were treated with 100 nM bafilomycin A1 (Cell Signaling, # 54645S) for 16 h prior to collection. For positive control, cells were treated with 10 μM mTOR inhibitor PP242 (Torkinib, SelleckChem #S2218) for 16 h prior to collection. At collection, cells were trypsinized and pipetted into a single-cell suspension and finally resuspended in 4% FBS in PBS. Samples were run on a Beckman Coulter Gallios 561 flow cytometer. Data were analyzed in FlowJo 10. Gating strategy included removal of non-transfected (i.e. GFP-/mCherry- cells) prior to analysis. Adherent and suspension conditions were performed in triplicate and the percentage of mCherry+/GFP- cells was analyzed in GraphPad Prism 8.

Caspase-Glo Assay. As previously described [7]. OVCAR4 cells grown in adherent and suspension conditions were used for a Caspase-Glo 3/7 assay (Promega). Luminescence was measured on a Promega GloMax Multi-detection System.

Gene signature TCGA Datasets: Gene-level expression data in the form of raw read counts were downloaded and merged from the TCGA database. Kidney cancer – KIRC and KIRP, colorectal cancer – COAD, breast cancer – BRCA, brain cancer – LGG, Skin cancer – SKCM, and ovarian cancer – OV. For each cohort, expression data were downloaded at the sample level and then merged by Ensembl gene ID. For quality purposes, genes in each of the data sets were filtered based on expression levels. For all data sets genes were retained if they had an average of at least 10 reads across all samples. Original data sets contained ~30,000 unique Ensembl gene IDs, and after filtering, all contained ~15,000 unique Ensembl gene IDs. For each cohort, to extract expression values for each of the candidate genes expected to predict survival, expression data was extracted based on matching gene names from the hg38 Ensembl annotation database. Expression data was further sub-setted to those genes within our candidate list based on Ensembl ID.

Modeling survival and generating Kaplan-Meier curves were done in 3 steps: 1) The first step was to fit a Cox proportional hazard model for each gene and extract the coefficient. 2) A gene signature score was calculated by taking the weighted sum of the candidate genes using the coefficient from step 1 as the respective weights. We then used the median of the gene signature distribution to divide the scores into high (above median) and low (below median) scores. 3) The dichotomous description of gene signature score (high or low gene signature score) was then used as a predictor to fit new Cox proportional hazard models and generate a Kaplan-Meier curve. P-values were taken from the log-likelihood statistic from the Cox proportional hazard models. With our gene signature we tested two-hypotheses: 1) do the expression levels of the top 108 genes predict survival? and 2) do the expression levels of 108 random genes predict survival better than the top 108 genes? The p-value used to determine significance in our survival analysis was set at $p < 0.05$. In addition, we randomly selected the same number of genes used in each original gene signature analysis and used this random gene set as our gene signature, permuted the expression and outcome and predicted survival. This was done 1000 times, and for each permuted data set we modeled survival as described for the original analysis, and generated a distribution of log-likelihood statistics. We then calculated p-values for each cohort's permutation analysis, which describes the proportion of times the permuted likelihood test was more extreme (i.e. more significant) than the log-likelihood generated from the original analysis. Our gene signature was significantly better at predicting survival than a random selection of 108 genes for those datasets with a permuted p-value < 0.05. CoxPH

models and Kaplan-Meier curves were generated using the survival [8] and *simPH* [9] packages. All analyses for the gene signature scores were performed in R (v3.5.1).

Publicly Available Data. We examined significant genes associated with metastatic disease in Tothill Ovarian Cohort and Bittner Ovarian Cohort. Differentially regulated genes ($p<0.05$) were identified from both dataset and cross-referenced the genes identified in the CRISPR/Cas9/RNA-seq comparison (Oncomine, ThermoFisher).

Statistical Analysis. Prism Graphpad (version 8) software was utilized to generate graphs. All statistical tests are two-sided unpaired t-test unless noted. Hypergeometric distribution was calculated using the following website: http://systems.crump.ucla.edu/hypergeometric/. A significance threshold was set at $p<0.05$.

Data and Software Availability. The accession number for the CRISPR/Cas9 screen and RNA-seq data reported is GSE123290.

Supplemental References

1. Abraham, C.G., et al., *DeltaNp63alpha Suppresses TGFB2 Expression and RHOA Activity to Drive Cell Proliferation in Squamous Cell Carcinomas.* Cell Rep, 2018. **24**(12): p. 3224-3236.
2. Yamamoto, T.M., et al., *Activation of Wnt signaling promotes olaparib resistant ovarian cancer.* Mol Carcinog, 2019.
3. Kim, D., B. Langmead, and S.L. Salzberg, *HISAT: a fast spliced aligner with low memory requirements.* Nat Methods, 2015. **12**(4): p. 357-60.
4. Gehrke, S., et al., *Metabolomics evaluation of early-storage red blood cell rejuvenation at 4 degrees C and 37 degrees C.* Transfusion, 2018. **58**(8): p. 1980-1991.
5. Wheeler, L.J., et al., *CBX2 identified as driver of anoikis escape and dissemination in high grade serous ovarian cancer.* Oncogenesis, 2018. **7**(11): p. 92.
6. Kimura, S., T. Noda, and T. Yoshimori, *Dissection of the autophagosome maturation process by a novel reporter protein, tandem fluorescent-tagged LC3.* Autophagy, 2007. **3**(5): p. 452-60.
7. Gordon, M.A., et al., *The long non-coding RNA MALAT1 promotes ovarian cancer progression by regulating RBFOX2-mediated alternative splicing.* Mol Carcinog, 2018.
8. Andersen, P.K. and R.D. Gill, *Cox's Regression Model for Counting Processes: A Large Sample Study.* The Annals of Statistics, 1982. **10**(4): p. 1100-1120.
9. Gandrud, C., *simPH: An R Package for Illustrating Estimates from Cox Proportional Hazard Models Including for Interactive and Nonlinear Effects.* 2015, 2015. **65**(3): p. 20.